

# On the Intrinsic Alignments of the Late-Type Spiral Galaxies from the Sloan Digital Sky Survey Data Release 7

Jounghun Lee

*Astronomy Program, Department of Physics and Astronomy, FPRD, Seoul National University,  
Seoul 151-747, Korea*

jounghun@astro.snu.ac.kr

## ABSTRACT

A robust detection of the tidally induced intrinsic alignments of the late-type spiral galaxies with high statistical significance is reported. From the spectroscopic galaxy sample of SDSS DR7 compiled by Huertas-Company et al. which lists each galaxy's probabilities of being in five Hubble types,  $P(E)$ ,  $P(Ell)$ ,  $P(S0)$ ,  $P(Sab)$ ,  $P(Scd)$ , we select the nearby large late-type spiral galaxies which have redshifts of  $0 \leq z \leq 0.02$ , probabilities of  $P(Scd) \geq 0.5$  and angular sizes of  $D \geq 7.92$  arcsec. The spin axes of the selected nearby large late-type spiral galaxies are determined up to the two-fold ambiguity with the help of the circular thin-disk approximation and their spatial correlations are measured as a function of the separation distance  $r$ . A clear signal of the intrinsic correlation as high as  $3.4\sigma$  and  $2.4\sigma$  is found at the separation distance of  $r \approx 1 h^{-1}\text{Mpc}$  and  $r \approx 2 h^{-1}\text{Mpc}$ , respectively. The comparison of this observational results with the analytic model based on the tidal torque theory reveals that the spin correlation function for the late-type spiral galaxies follow the quadratic scaling of the linear density correlation and that the intrinsic correlations of the galaxy spin axes are stronger than that of the underlying dark halos. We investigate a local density dependence of the galaxy spin correlations and found that the correlations are stronger for the galaxies located in dense regions having more than 10 neighbors within  $2 h^{-1}\text{Mpc}$ . We also attempt to measure a luminosity dependence of the galaxy spin correlations, but find that it is impossible with our magnitude-split samples to disentangle a luminosity from a redshift dependence. We provide the physical explanations for these observational results and also discuss the effects of possible residual systematics on the results.

*Subject headings:* cosmology:theory — methods:statistical — large-scale structure of universe

## 1. INTRODUCTION

The building blocks of the large-scale structure in the universe are the galactic dark halos that are believed to underlie the luminous galaxies. Although the galactic dark halos are not directly

observable, their intrinsic properties can be inferred and estimated from the galaxy observables such as luminosity, color, morphology and spatial correlations. For instance, how luminous a given galaxy is related to how massive its underlying dark halo is. The colors and morphologies of the observed galaxies reflect the formation epochs and assembly history of their galactic halos. Finding the hidden relations between the galaxy observables and intrinsic properties of the underlying dark halos is one of the most important tasks in the field of the large-scale structure.

The directions of the galaxy angular momentum (i.e., the galaxy spin axes) are one of those galaxy observables that are believed to have a direct connection with the intrinsic properties of the underlying dark halos. In the standard linear tidal torque theory (Peebles 1969; Doroshkevich 1970; White 1984; Dubinski 1992; Catelan & Theuns 1996), the tidal torques from the surrounding matter originate the angular momentum of the proto-galactic halos in the linear regime (see Schäfer 2009, for a recent review). In consequence, the directions of the angular momentum of the proto-galactic halos come to be aligned with the intermediate principal axes of the local tidal tensors (Lee & Pen 2000, 2001, 2002; Porciani et al. 2002). As the tidal fields are spatially correlated, the correlations between the spin axes of the proto-galactic halos and the principal axes of the local tidal tensors would induce the spatial correlations of the spin axes of the proto-galactic halos. A detailed analysis have shown that the spatial correlations of the spin axes of the galactic halos would follow a quadratic scaling with the two point correlation function of the linear density field provided that the linear tidal torque theory is valid (Pen et al. 2000; Sugerman et al. 2000; Lee & Pen 2001; Crittenden et al. 2001).

A critical question is whether or not the tidally induced initial correlations between the spin axes of the galactic halos have been retained to a detectable level and how strong the retained correlations are. If the intrinsic correlations of the spiral galaxies are detected and if we can model them well with the tidal torque theory, it would make it plausible to reconstruct the initial tidal fields from the observable spin fields as proposed by Lee & Pen (2000). Furthermore, it would have a direct impact on the weak lensing community where the intrinsic alignments of the spiral (or blue) galaxies are often assumed to be zero (e.g, Joachimi et al. 2010; Mandelbaum et al. 2010).

Plenty of observational efforts have so far been made to address this issue. Pen et al. (2000) measured the spatial correlations of the spin axes of the nearby spiral galaxies from the Tully catalog and reported a tentative detection of  $2\sigma$  signals. They claimed that the observed trend of the galaxy spin correlations is consistent with the quadratic scaling of the linear density two-point correlations. Lee & Pen (2002) searched directly for the correlations between the spin axes of the nearby spiral galaxies and the intermediate principal axes of the tidal fields using the data from the Point Source Galaxy catalog (Saunders et al. 2000).

Brown et al. (2002) demonstrated that the intrinsic shape correlations of the elliptical galaxies from the SuperCOSMOS survey (Hambly et al. 2001) are consistent with the quadratic scaling with the linear density correlations under the assumption that the projected minor axes of the observed elliptical galaxies are orthogonal to the projected spin axes of their underlying halos. Navarro et. al.

(2004) noted that the distribution of the inclination angles of the nearby disk galaxies relative to the Supergalactic plane is consistent with the prediction of the linear tidal torque theory. Trujillo et al. (2006) claimed that the observed alignments of the galaxies in the vicinity of large voids are well explained by the tidally induced intrinsic correlations. Lee & Erdoğdu (2007) detected a  $2\sigma$  signal of the correlations between the spin axes of the nearby spiral galaxies from the Tully catalog and the intermediate principal axes of the local tidal field constructed from the 2MASS redshift survey (Erdoğdu et al. 2006, and references therein).

Lee & Pen (2007) measured the two dimensional projected spin correlations of the blue galaxies from the Sloan survey (York et al. 2000) and found a  $3\sigma$  signal at one single distance bin of  $r \sim 1 h^{-1}\text{Mpc}$ . Paz et al. (2008) found the correlations between the galaxy angular momentum vectors and the large-scale structures from the Sloan survey and claimed that their results are in qualitative agreement with the predictions of the tidal torque theory. Slosar et al. (2009) reported a first detection of the chiral correlations of nearby galaxies. Recently, Jones et al. (2010) found that the spin axes of the spiral galaxies in the filaments tend to be aligned with the major axes of the filaments and concluded that the observed spin alignments of the filament galaxies provide a fossil evidence for the tidally-induced intrinsic correlations.

In spite of these observational evidences, it is still inconclusive whether or not the present galaxies still retain its initially memory of the tidally induced intrinsic spin correlations for the following two reasons. The first reason is that the reported correlation signals are not strong enough to be confirmed as true signals. For instance, the galaxy spin correlation signals reported by Pen et al. (2000), Lee & Pen (2001) and Lee & Erdoğdu (2007) are significant only at  $2 - 2.5\sigma$  levels. The samples on which the analyses of Navarro et al. (2004) and Trujillo et al. (2006) were based are so small that their conclusions suffer from poor number statistics. Furthermore, there have reported some counter evidences against the existence of the intrinsic galaxy alignments. For example, Aryal & Saurer (2005) searched for the alignments of the spin vectors of the galaxies in Abell clusters but failed in finding any signals.

As for the strong correlations of the projected major axes of the elliptical galaxies measured by Brown et al. (2002), although it is good number statistics, the signals suffer from large uncertainties associated with regarding the projected major axes of the elliptical galaxies as the directions orthogonal to the spin axes of the underlying dark halos. True as it is that the minor axes of the elliptical galaxies should be more or less aligned with the spin axes of their underlying dark halos (e.g., Bailin et al. 2005; Bailin & Steinmetz 2005), their spatial correlations are not so good tracers of the linear tidal fields as the spin correlations of the spiral galaxies, since the shapes of the elliptical galaxies are apt to be affected by the subsequent processes such as the anisotropic merging/infall, galaxy-galaxy interactions and etc (e.g., Fuller et al. 1999). Thus, the best targets for the measurement of the tidally-induced intrinsic alignments are the spiral galaxies and their spin orientations.

The second reason comes from the concerns about spurious signals that could be produced by

systematics. There are three major sources for the systematics in the measurement of the intrinsic correlations of the galaxy spin axes: the weak gravitational lensing effect, presence of thick central bulges and inaccurate measurements of the spin axes in case that the galaxies have small angular sizes. It has been known that the extrinsic alignments of the galaxy shapes due to the weak gravitational lensing effect would create spurious signals of the spin-spin correlations of the spiral galaxies (or ellipticity-ellipticity correlations of the elliptical galaxies) at redshifts  $z \geq 0.1$  (e.g., Pen et al. 2000; Croft & Metzler 2000; Heavens et al. 2000; Catelan et al. 2001; Crittenden et al. 2001, 2002; Jing 2002; Mackey et al. 2002; Heymans & Heavens 2003; Hirata & Seljak 2004; Hirata et al. 2004; Mandelbaum et al. 2006; Hirata et al. 2007; Joachimi & Bridle 2010). The presence of thick central bulges in the spiral galaxies could cause significant systematics since it invalidates the circular thin-disk approximation which is almost exclusively used to measure the orientations of the galaxy spin axes. In case that the galaxies have small angular sizes, their position angles and axial ratios would be difficult to measure accurately, which would propagate into the systematic errors in the measurement of the galaxy spin axes.

The errors caused by the above three systematics in the measurement of the intrinsic correlations can be minimized if one selects only the large late-type spiral galaxies (of Hubble types Scd) observed at lowest redshifts. Using only low- $z$  galaxies, one can reduce the weak gravitational lensing effect to a completely negligible level. Selecting only large late-type spiral galaxies which have the smallest central bulges, one can guarantee that the measurements of the spin axes through the circular thin disk approximation are reliable. To select such galaxies from the observational data, however, it is necessary to have information on the spectroscopic redshifts and Hubble types of the observed galaxies. Very recently, Huertas-Company et al. (2010) have released a catalog of the galaxies from the Sloan Digital Sky Survey Data Release 7 (SDSS DR7), in which such information are all available. Our goal here is to measure the true intrinsic correlations of the nearby large late-type spiral galaxies from this catalog and to study their behaviors and their dependence on the local density and luminosity.

The organization of this Paper is as follows. In §2.1, the sample of the nearby large late-type galaxies selected from the SDSS DR7 is described and the number distributions of the selected galaxies as a function of their magnitude and local density are derived. In §2.2, it is explained how the spin axes of the selected galaxies are determined up to two-fold degeneracy with the help of the circular thin disk approximation. In §3.1, the correlations between the spin axes of the selected nearby large Scd galaxies are measured and the bootstrap error analysis is presented. In §3.2 the dependence of the galaxy spin correlations on local density and luminosity is investigated. In §3.3 the possible residual systematics are discussed and its effect is examined. In §4, the observational results are compared with the analytic models based on the tidal torque theory and the bestfit parameters to quantify the strengths of the correlations are determined. In §5, the results are summarized and a conclusion is drawn.

## 2. PROPERTIES OF THE LATE-TYPE SPIRAL GALAXIES FROM SDSS DR7

### 2.1. Selection of the Nearby Large Scd Galaxies

The galaxy catalog compiled by Huertas-Company et al. (2010) consists of a total of 698420 galaxies in redshift range of  $0 \leq z \leq 0.16$  from the SDSS DR7 (Abazajian et al. 2009). It provides information on spectroscopic redshift ( $z$ ), right ascension ( $\alpha$ ), declination ( $\delta$ ) and the probabilities of being in the five morphological classes (E, Ell, S0, Sab, Scd) for each galaxy. Through private communication with M. Huerta-Company, we obtain additional information on the major and minor axes, position angle ( $\vartheta_P$ ) and r-band model magnitude ( $m_r$ ) of each galaxy in the catalog.

To minimize the systematics in the measurement of the spatial correlations of the galaxy spin axes, we select only those galaxies which have redshifts in the range of  $0 \leq z \leq 0.02$ , probability of being in the morphological class of Scd higher than 0.5, and angular size (given as the major axis length)  $D$  larger than 7.92 arcsec (corresponding to 20 pixels in the SDSS frames). A total of 4065 galaxies from the catalog are found to satisfy these three conditions. Figure 1 plots the number distribution of the galaxies from the catalog as a function of its probability of being in the Scd morphological class,  $P(\text{Scd})$ . The results shown in each panel is drawn under the condition of  $0 \leq z \leq 0.02$  (top left panel);  $0 \leq z \leq 0.02$  and  $P(\text{E}) \leq P(\text{S0}) \leq P(\text{Sab}) \leq P(\text{Scd})$  (top right panel);  $0 \leq z \leq 0.02$  and  $P(\text{Scd}) \geq 0.5$  (bottom left panel);  $0 \leq z \leq 0.02$ ,  $P(\text{Scd}) \geq 0.5$  and  $D \geq 7.92$  arcsec (bottom right panel). Using information on  $z$ ,  $\alpha$  and  $\delta$ , we determine the comoving distance to each galaxy in unit of  $h^{-1}\text{Mpc}$  assuming a WMAP7 cosmology (Komatsu et al. 2010).

To determine the local density of the selected galaxies, we first construct a volume-limited sample of the galaxies (regardless of their types) in the same redshift range from the SDSS spectroscopic data. Basically, the volume-limited sample includes only those SDSS galaxies whose apparent  $r$ -band magnitudes would exceed a given flux limit,  $m_{r,c}$ , if placed at  $z = 0.02$ . Figure 3 plots the fraction of the SDSS galaxies included in a volume-limited sample as a function of  $m_{r,c}$ . When the SDSS flux limit value of  $m_{r,c} = 15.2$  is applied, a total of 12273 galaxies are found to belong to the constructed volume-limited sample. Now, for each selected nearby Scd galaxy from the catalog provided by Huertas-Company et al. (2010), we count the number of its neighbor galaxies from the volume-limited sample whose separation distance from the given selected Scd galaxy is less than  $r_s = 2 h^{-1}\text{Mpc}$ . Figure 2 plots the number distribution of the selected nearby large Scd galaxies as a function of the neighbor galaxies located within separation of  $r_s$ . The distribution has its maximum at  $N_{ng} \approx 10$  and only a small fraction of the selected Scd galaxies have indeed more than 100 neighbor galaxies within  $r_s$ . It indicates that the majority of the selected nearby Scd galaxies are field galaxies, not belonging to galaxy clusters.

With the measured comoving distance to each galaxy, we convert each galaxy’s apparent magnitude  $m_r$  to the absolute magnitude  $M_r$  by using the system of the inverse hyperbolic sine magnitudes (asinh) (Lupton et al. 1999). Figure 4 plots the number distribution of the selected nearby large Scd galaxies as a function of  $M_r$ . Table 1 lists the redshift range, the total number,

mean absolute r-band magnitude and mean number of the neighbors within  $2 h^{-1}\text{Mpc}$ , averaged over all the selected nearby large Scd galaxies.

## 2.2. Determination of the Galaxy Spin Axes

To determine the spin axes of each selected galaxy, we use information from the SDSS imaging data on galaxy's axial ratio  $q$  and position angle  $\vartheta_P$  which were extracted by the SDSS team from the coefficients of the Fourier expansion of the 25 magnitudes per square arcsecond isophote measured in the  $r$ - band. Placeholders for the errors on each of these quantities were not available from the website (<http://www.sdss.org/dr7>). We calculate the inclination angle,  $\xi$ , of each selected galaxy as (Haynes & Giovanelli 1984)

$$\cos^2 \xi = \frac{q^2 - p^2}{1 - p^2}. \quad (1)$$

where  $p$  is the intrinsic flatness parameter that depends on the galaxy morphological type. Here, we adopt the value of  $p = 0.10$  for the Scd galaxies, given by Haynes & Giovanelli (1984). If the inclination angle of a given galaxy in the selected sample is less than the intrinsic flatness parameter (i.e.,  $q \leq p$ ), then we set it at  $\pi/2$  (see §3.3 for discussion on the systematics related to the intrinsic flatness parameter).

With the help of the circular thin-disk approximation and given information on the inclination angle  $\xi$  and position angle  $\vartheta_P$ , we determine the unit spin vector,  $\hat{\mathbf{L}}$ , of each selected nearby Scd galaxy in a local spherical-polar coordinate system up to sign-ambiguity of the radial component as (Lee & Erdoğdu 2007)

$$\hat{L}_r = \pm \cos \xi, \quad (2)$$

$$\hat{L}_\theta = (1 - \cos^2 \xi)^{1/2} \sin \vartheta_P, \quad (3)$$

$$\hat{L}_\phi = (1 - \cos^2 \xi)^{1/2} \cos \vartheta_P \quad (4)$$

where  $\hat{L}_r$ ,  $\hat{L}_\theta$ ,  $\hat{L}_\phi$  correspond to the radial, polar and azimuthal component of  $\hat{\mathbf{L}}$ , respectively. This sign-ambiguity in the radial components of  $\hat{\mathbf{L}}$  is due to the fact that one cannot determine whether the rotation of a given galaxy upon its symmetry axis is clock-wise or counter-clock wise (Pen et al. 2000).

Using information on the equatorial coordinates,  $(\alpha, \delta)$ , we determine the unit spin vector of each selected Scd galaxy in the Cartesian coordinate system up to two-fold degeneracy as

$$\hat{L}_{a1} = \hat{L}_r \sin \theta \cos \phi + \hat{L}_\theta \cos \theta \cos \phi - \hat{L}_\phi \sin \phi, \quad (5)$$

$$\hat{L}_{a2} = \hat{L}_r \sin \theta \sin \phi + \hat{L}_\theta \cos \theta \sin \phi + \hat{L}_\phi \cos \phi, \quad (6)$$

$$\hat{L}_{a3} = \hat{L}_r \cos \theta - \hat{L}_\theta \sin \theta, \quad (7)$$

$$\hat{L}_{b1} = -\hat{L}_r \sin \theta \cos \phi + \hat{L}_\theta \cos \theta \cos \phi - \hat{L}_\phi \sin \phi, \quad (8)$$

$$\hat{L}_{b2} = -\hat{L}_r \sin \theta \sin \phi + \hat{L}_\theta \cos \theta \sin \phi + \hat{L}_\phi \cos \phi, \quad (9)$$

$$\hat{L}_{b3} = -\hat{L}_r \cos \theta - \hat{L}_\theta \sin \theta, \quad (10)$$

where  $\theta = \pi/2 - \delta$  and  $\phi = \alpha$ . Finally, to each selected nearby Scd galaxy, we assign a set of two unit spin vectors,  $\hat{\mathbf{L}}_a$  and  $\hat{\mathbf{L}}_b$ , which differ from each other by the sign of  $\hat{L}_r$  (Pen et al. 2000).

### 3. INTRINSIC SPIN CORRELATIONS OF THE LATE-TYPE SPIRAL GALAXIES

#### 3.1. Measurement of the Galaxy Spin Correlations

The spatial correlation of the galaxy spin axes is defined by Pen et al. (2000) as

$$\eta(r) \equiv \langle |\hat{\mathbf{L}}(\mathbf{x}) \cdot \hat{\mathbf{L}}(\mathbf{x} + \mathbf{r})|^2 \rangle - \frac{1}{3}. \quad (11)$$

Here the ensemble average is taken over those galaxy pairs whose separation distance is in a differential range of  $[r, r + dr]$ . The value of  $1/3$  is subtracted since it is the value of the ensemble average when there is no correlation. In practice, however, due to the two-fold degeneracy in the determination of  $\hat{\mathbf{L}}$ , the correlation  $\eta(r)$  can be measured only as (Pen et al. 2000)

$$\eta(r) = \frac{1}{4} \left( \langle |\hat{\mathbf{L}}_a \cdot \hat{\mathbf{L}}'_a|^2 \rangle + \langle |\hat{\mathbf{L}}_a \cdot \hat{\mathbf{L}}'_b|^2 \rangle + \langle |\hat{\mathbf{L}}_b \cdot \hat{\mathbf{L}}'_a|^2 \rangle + \langle |\hat{\mathbf{L}}_b \cdot \hat{\mathbf{L}}'_b|^2 \rangle \right) - \frac{1}{3} \quad (12)$$

where  $\hat{\mathbf{L}}'$  represents the unit spin vector measured at  $\mathbf{x} + \mathbf{r}$ .

For all pairs of the galaxies, we calculate the squares of the dot products of their unit spin vectors, taking into account the two-fold degeneracy. Binning the separation distances  $r$ , we take the ensemble average over those pairs whose separation distances belong to a certain distance bin and subtract  $1/3$  to determine  $\eta(r)$  in accordance with Equation (12). Although we try to reduce systematic errors as much as possible through constraining the redshift-range, morphology and angular size, there could be some residual systematics. To sort out possible residual systematics, we perform a bootstrap error analysis. The spin correlation functions,  $\eta(r)$ , are remeasured from each of the 1000 bootstrap resamples which is constructed through shuffling randomly the positions of the selected galaxies. The bootstrap errors,  $\sigma_b$ , are calculated as  $\sigma_b \equiv \langle (\eta - \bar{\eta}_b)^2 \rangle^{1/2}$  where the ensemble average is taken over the 1000 resamples and  $\bar{\eta}_b$  represents the bootstrap mean. If there were no residual systematics in the measurement of the galaxy spin axes, then the bootstrap mean value would be very close to zero. The degree of the deviation of the bootstrap mean from zero would indicate the level of the residual systematics.

Figure 5 plots the observed galaxy spin correlations for four different cases of the galaxy angular size cut ( $D_c = 0.00, 1.98, 3.96$  and  $7.92$  arcsec in the top-left, top-right, bottom-left and bottom-right panel, respectively). In each panel the error bars represent one standard deviation,

$\sigma_\eta$ , in the measurement of  $\eta(r)$ . The thin solid and dashed line in Figure 5 represents the bootstrap mean  $\bar{\eta}_b$  and bootstrap errors,  $\sigma_b$ , respectively, while the thin dotted line corresponds to the zero signal. As it can be seen, a clear signal as strong as  $3.4\sigma_b$  is detected for all four cases of  $D_c$  at the second radial bin corresponding to the distance of  $r \approx 1.25h^{-1}\text{Mpc}$ . For the cases of  $D_c = 0$  and  $1.98$  arcsec, the third radial bins corresponding to  $r \approx 2h^{-1}\text{Mpc}$  also exhibit a  $3\sigma_b$  signal while for the other two cases of  $D_c = 3.96$  and  $7.92$ , the correlation at  $r = 2h^{-1}\text{Mpc}$  diminishes down to  $2.4\sigma_b$  level.

As mentioned in §1, for the galaxies having small angular sizes the spin axes are difficult to measure accurately. As it can be seen from Figure 5, for the two cases of  $D_c = 0$  and  $1.98$  arcsec where the small angular size galaxies are included, the mean bootstrap values (thin solid line) show non-negligible deviations from zero (larger than  $10^{-4}$ ). Thus, the  $3\sigma_b$  signals detected at  $r \approx 2h^{-1}\text{Mpc}$  for these two cases are likely to be contaminated by the systematics. Figure 6 shows more clearly how the averaged bootstrap mean value changes with  $D_c$ . As it can be seen, the bootstrap mean value decreases as  $D_c$  increases and drops below  $10^{-4}$  (negligible level) when  $D_c$  reaches up to  $7.92$  arcsec, which justify our choice of  $D_c = 7.92$  arcsec for this analysis.

Since the correlation function,  $\eta(r)$ , is computed as a function of the three dimensional separation, there may be some cross-correlations at different radii. If the cross-correlations between the second and third radial bins are significant, then the signal detection for the second radial bin would have lower significance. To quantify the amount of cross-correlations, we compute the covariance matrix,  $C_{ij}$ , that is defined

$$C_{ij} \equiv \langle (\eta_i - \bar{\eta}_{bi})(\eta_j - \bar{\eta}_{bj}) \rangle \quad (13)$$

where the ensemble average is taken over 1000 bootstrap resamples,  $\eta_i$  is the correlation at the  $i$ -th bin from a bootstrap resample, and  $\bar{\eta}_{bi}$  is the bootstrap mean at the  $i$ -th bin. If the cross-correlations between the second and third radial bins are significant, then the off-diagonal component,  $C_{23}$ , would be comparable in magnitude to the diagonal component,  $C_{22}$ . It is found that  $C_{22} = 3.18 \times 10^{-6}$  while  $C_{23} = -0.17 \times 10^{-7}$ . This implies that the cross-correlations between the second and third radial bins are order of magnitude smaller (and even negative) than the correlations at the second radial bins, which proves that the signal detected at the second radial bin is robust.

### 3.2. Dependence on Local Number Density and Luminosity

Now that we have detected non-zero galaxy spin correlations from the SDSS data, we would like to investigate whether or not  $\eta(r)$  depends on the local number density  $N_{ng}$  of neighbor galaxies. Applying the number density cut,  $N_{ng,c} = 10$ , to the sample, we divide the selected Scd galaxies into two subsamples each of which consists of those nearby large Scd galaxies with  $N_{ng} \leq N_{ng,c}$  and  $N_{ng} > N_{ng,c}$ , respectively. Then, we measure  $\eta(r)$  from each subsample separately, the results of which are plotted in the top and bottom panel of Figure 7, respectively.

As it can be seen, for the subsample with  $N_{ng} > 10$ , we find a correlation signal as significant as  $3.1\sigma_b$  signal at  $r \approx 1.25 h^{-1}\text{Mpc}$ , while for the subsample with  $N_{ng} \leq 10$ , no correlation signal is detected. The bootstrap mean values are quite close to zero for both of the cases, which indicates that the detected signal is not spurious. This result shows that those Scd galaxies located in denser regions tend to have stronger spin correlations. A possible physical explanation is that the galaxies located in denser regions experience so stronger tidal forces from the surrounding neighbor mass distribution that the tidally-induced intrinsic correlations of their spin axes are better retained, which is consistent with the previous results of Lee & Erdogdu (2007).

Using the galaxy pairs in which one galaxy has  $N_{ng} > N_{ng,c}$  and the other has  $N_{ng} \leq N_{ng,c}$ , we also measure the cross-correlations of the spin axes between the two subsamples, the result of which is plotted in Figure 8. As one can see, the result is consistent with zero cross-correlation, which reveals that the spin axes of the galaxies in less dense regions are not correlated with those of the galaxies in denser regions.

To investigate how the intrinsic correlations depend on the luminosity, we take the median  $r$ -band absolute magnitude,  $-16.67$ , as the threshold  $M_{r,c}$ , and divide the selected galaxies into two subsamples each of which consists of those nearby large Scd galaxies with  $M_r > -16.67$  and  $M_r \leq -16.67$ , respectively. Then, we measure  $\eta(r)$  from each subsample separately, which are plotted in the top and bottom panel of Figure 9, respectively. As it can be seen, the correlation function,  $\eta(r)$ , exhibits a  $4.9\sigma_b$  peak at  $r \approx 1.25 h^{-1}\text{Mpc}$  and a  $2.4\sigma_b$  peak at  $r \approx 2 h^{-1}\text{Mpc}$  in the fainter and brighter galaxy sample, respectively.

This result, however, cannot be interpreted as a clear luminosity dependence of the galaxy spin correlations. In fact, the peaks of  $\eta(r)$  detected at  $1.25 h^{-1}\text{Mpc}$  and  $2 h^{-1}\text{Mpc}$  (for the fainter and brighter sample, respectively) turn out to correspond to a similar angular separation of galaxy pairs. It indicates the existence of significant residual systematics, which is also manifest from the relatively high degree of the deviation of the bootstrap mean from zero for the fainter sample as shown in the top panel of Figure 9. Furthermore, the redshift distributions of the two subsamples are found to be largely different: the brighter (fainter) sample is biased to relatively higher (lower) redshifts, as shown in Figure 10. The mean and median redshifts of the two subsamples are also listed in Table 2. Given that there should exist significant systematics and that it is impossible to disentangle a luminosity from a redshift dependence of the galaxy spin correlations, we admit that a luminosity dependence of the galaxy spin correlations cannot be measured with our magnitude-split samples.

In §3.3, we discuss fully the possible sources of this residual systematic errors involved in the measurement of the spin correlations of the fainter galaxies. Before moving on to the discussion on systematics, we also measure the spin cross correlations between the fainter and brighter samples, the result of which is plotted in Figure 11. As can be seen, a strong anti-correlation of the spin axes as significant as  $3\sigma_b$  is found at  $r \approx 10 h^{-1}\text{Mpc}$ . In other words, the spin axes of the fainter galaxies tend to be orthogonal to that of the brighter galaxies separated by the distance of  $\sim$

$10 h^{-1}\text{Mpc}$ . Given the numerical and observational results from the previous works (Bailin et al. 2005; Bailin & Steinmetz 2005; Jones et al. 2010; Hahn et al. 2010), we explain this observational result as follows: The spin axes of the fainter galaxies are aligned with the intermediate principal axes of the local tidal fields as predicted by the linear tidal torque theory. Whereas for the brighter galaxies which are usually located in cosmic filaments, their spin axes tend to be aligned with the longest axes of the local filaments, i.e., the minor principal axes of the local tidal fields (Jones et al. 2010), as revealed by the recent numerical results from hydrodynamic simulations (Hahn et al. 2010). In consequence, the two subsamples have strong anti spin-correlations between each other. The separation distance of  $10 h^{-1}\text{Mpc}$  at which the strong anti-correlations are detected should be the typical separation between the faint isolated and bright wall galaxies.

### 3.3. Discussion on Systematics

For the accurate measurement of the galaxy spin correlations, we have tried to eliminate systematic errors as much as we can by constraining the redshift, morphological type and angular size of the SDSS galaxies. The small bootstrap errors shown in the bottom right panel of Figure 5 suggests that no severe systematics be existent in our constrained sample, and thus that our detection of the spin correlations be robust. Nevertheless, it has to be admitted that our results may not be completely free from systematics.

A possible source of residual systematics could be related to the constant value of the intrinsic flatness parameter,  $p = 0.1$  in Equation (1) that we adopt in accordance with Haynes & Giovanelli (1984) to account for the finite thickness of the Scd galaxies. Given that this value of  $p = 0.1$  was obtained by Haynes & Giovanelli (1984) from a sample of HI 21cm observations and that the shape of the neutral hydrogen distribution does not necessarily coincide with the optical shape of a galaxy, one may suspect that a different value of  $p$  should be used for the galaxies from the optical SDSS survey. An ideal way would be to look at the individual images of the optical shapes of the SDSS galaxies and to search for the optimal value to  $p$  for the selected Scd galaxies. This task, however, would be extremely time consuming and thus should be beyond the scope of this paper.

Instead, we inspect how the final results would change as we use different values to  $p$  in Equation (1). Haynes & Giovanelli (1984) explained that unless a galaxy has a well developed bulge like the early type spirals, the intrinsic flatness parameter must have the value in range of  $0.1 \leq p \leq 0.15$ . Since we select only Scd galaxies which optical shapes must have the thinnest bulges, we expect that the value of  $p$  would not differ significantly from 0.1. Figure 12 plots the same as Figure 5 but for four different cases of the intrinsic flatness parameter ( $p = 0.00.050.1$  and  $0.15$ ). As one can see, the final results change less than 10% as the value of  $p$  changes from 0. to 0.15, which justify our choice of  $p = 0.1$ .

Another possible source of residual systematics is the limitation of the circular disk approximation. The morphology class of Scd from the SDSS catalog includes the irregular galaxies

(Huertas-Company et al. 2010), for which the circular thin disk approximation would be invalid. But, through private communication with M.Huertas-Company, we have learned that the fraction of the included irregular galaxies must be small since the irregular galaxies are usually fainter while the targets of the spectroscopic SDSS sample are brighter. The relatively larger bootstrap mean values of  $\eta(r)$  for the fainter samples shown in the top panel of Figure 9 are most likely to be caused by the inaccurate measurement of the spin axes of the irregular galaxies that are included in the subsample of the fainter galaxies ( $M_r > -16.67$ ). An ideal way should be to look at the individual images of the fainter galaxies and sort out the irregular galaxies from the fainter sample. However, it would be also extremely time consuming and thus should be beyond the scope of this paper. Here, we just state explicitly that the residual systematics could cause spurious signals of correlations for the fainter Scd galaxy sample, which is most likely to be due to the limitation of the circular thin disk approximation and that a better algorithm for the measurement of the spin axes of the irregular galaxies would be desirable.

## 4. COMPARISON WITH THE THEORETICAL MODEL

### 4.1. A Brief Review of the Analytic Model

According to the linear tidal torque theory, the angular momentum vector of a proto-galactic halo  $\mathbf{L} = (L_i)$  is expressed in terms of the proto-galaxy inertia momentum tensor  $\mathbf{I} = (I_{ij})$  and the local tidal shear tensor  $\mathbf{T} = (T_{ij})$  (Doroshkevich 1970; White 1984; Catelan & Theuns 1996; Lee & Pen 2000, 2001; Crittenden et al. 2001; Lee & Pen 2002; Porciani et al. 2002; Lee & Erdogdu 2007; Lee & Pen 2008)

$$L_i \propto \epsilon_{ijk} T_{jl} I_{lk}, \quad (14)$$

where  $\epsilon_{ijk}$  is the fully anti-symmetric tensor. Equations (14) implies that the spin axes of the proto-galaxies (i.e., the direction of the proto-galaxy angular momentum vector) are not random but correlated with the intermediate principal axes of the local tidal field tensors (Catelan & Theuns 1996; Lee & Pen 2000). Assuming that the initially generated correlations between  $\mathbf{L}$  and  $\mathbf{T}$  have been retained to some non-negligible degree till present epoch, Lee & Pen (2000) have proposed the following formula to quantify the strength of the correlations:

$$\langle \hat{L}_i \hat{L}_j \rangle = \frac{1+a}{3} \delta_{ij} - a \hat{T}_{ik} \hat{T}_{kj}, \quad (15)$$

where  $\hat{\mathbf{L}}$  is the unit spin vector of a given galaxy,  $\hat{\mathbf{T}}$  is the unit traceless tidal shear tensor smoothed on the galactic scale, and  $a$  is a free parameter to quantify the strength of the correlations between  $\hat{\mathbf{L}}$  and  $\hat{\mathbf{T}}$ .

A direct application of Equation (15) to the spatial correlations between the spin axes of neighbor galaxies have yielded the following formula for the galaxy spin-spin correlations (Pen et al.

2000; Lee & Pen 2001; Crittenden et al. 2001)

$$\eta(r) \approx \frac{a^2 \xi^2(r; R)}{6 \xi^2(0; R)}, \quad (16)$$

where  $\xi(r)$  is the two-point correlations of the linear density field smoothed on the galactic scale ( $R \approx 1 h^{-1}\text{Mpc}$ ) (e.g., see Bardeen et al. 1986). According to Equation (16), the spatial correlations between the galaxy spin axes would follow a quadratic scaling of the density correlation, decreasing rapidly to zero as  $r$  increases. We fit the observations results obtained in §3.1 and 3.2 to Equation (16) to determine the best-fit correlation parameter,  $a$  and examine whether or not the observed spin correlations follow the quadratic scaling with the linear density correlation,  $\xi(r)$ .

#### 4.2. Observed Scaling of the Galaxy Spin-Spin Correlations

We minimize the following generalized  $\chi^2$  to find the bestfit-value of  $a$  (Hartlap et al. 2007).

$$\chi^2 \equiv \frac{1}{(N_{bin} - 1)} [\eta_i - \eta(r_i)] C_{ij}^{-1} [\eta_j - \eta(r_j)], \quad (17)$$

where  $C_{ij}^{-1}$  is the inverse of  $C_{ij}$  that is defined in Equation (13),  $\eta(r_i)$  represents the theoretical value calculated at the  $i$ -th distance bin,  $\eta_i$  is the observed correlation at the same distance bin (with the bootstrap means subtracted) and  $N_{bin}$  is the number of radial bins. Note that since there is only one parameter, the degree of freedom for  $\chi^2$  is given as  $N_{bin} - 1$ . Here, the covariance matrix  $C_{ij}$  is computed using the bootstrap resamples as defined in §2.2 and the fitting is done for the distance range of  $0.5 \leq r/(h^{-1}\text{Mpc}) \leq 50$  since at larger distances the numerical flukes tend to contaminate the fitting. If this *reduced*  $\chi^2$  have a value close to unity, the theoretical model, Equation (16), would be regarded as a good fit to the observational result.

Figure 13 plots the best-fit model as solid line and compares it with the observational results (square dots). The best-fit value of  $a$  is found to be  $0.25 \pm 0.04$  and the corresponding value of  $\chi^2$  is found to be 0.83 (see Table 3). Here, the error associated with the measurement of  $a$  is determined as (Hartlap et al. 2007)

$$\sigma_a^2 = \left( \frac{d^2 \chi^2}{da^2} \right)^{-1} \quad (18)$$

Now that the reduced  $\chi^2$  is found to be close to unity and the best-fit value of  $a$  is found to be  $6\sigma_a$  higher than zero, it can be said that the observed spin correlations are indeed tidally induced, having quadratic scaling with the linear density correlations, as predicted by the linear tidal torque theory.

We note here that both of the best-fit value of  $a$  are larger than that determined by Lee & Pen (2008) through fitting of the numerical data from the Millennium Run simulations (see Table 3 in Lee & Pen 2008). There are two important implications of this result. First of all, the spin orientations of the luminous galaxies may not be perfectly aligned with those of their dark halos,

which is consistent with the previous numerical results (e.g., Bailin et al. 2005; Bailin & Steinmetz 2005; Hahn et al. 2010). Second of all, the luminous galaxies have retained better the initial memory of the tidally induced intrinsic spin-spin correlations than their dark halos. This phenomenon may be explained as follows. The luminous galaxies are located in the inner parts of the galactic halos while the dark matter particles are stretched to the outer parts of the dark halos (e.g., Bailin & Steinmetz 2005; Hahn et al. 2010). Therefore, the spin orientations of the luminous galaxies may be less vulnerable than those of their dark counterparts to the destructive nonlinear effects from the surroundings which would break the tidally induced intrinsic correlations.

The fitting results for the subsamples with  $N_{ng} > 10$  and  $M_r > -16.67$  are also plotted in Figures 14 and 15, respectively. The best-fit values of  $a$  and the minimum value of  $\chi^2$  corresponding to these two cases are also listed in the second and third rows of Table 3. As one can see, for the case of  $N_{ng} > 10$ , the best-fit value of  $a$  has the largest value, approximately 0.34. As mentioned in §3.2, it may be due to the stronger tidal forces from the surrounding.

## 5. SUMMARY AND CONCLUSIONS

Selecting those large nearby late-type spiral galaxies which have angular sizes larger than 7.92 arcsec, low redshifts ( $0 \leq z \leq 0.02$ ), and morphological type of Scd from the SDSS DR7, and we have measured the spatial correlations between their spin axes. The summary of our results is the following.

- A clear signal of the intrinsic correlation as strong as  $3.4\sigma_b$  and  $2.4\sigma_b$  (where  $\sigma_b$  is the bootstrap error) is detected at  $r \approx 1.25 h^{-1}\text{Mpc}$  and  $r \approx 2.0 h^{-1}\text{Mpc}$ , respectively. The cross-correlations between the two radial bins are found to be insignificant.
- The galaxies having more than ten neighbors within separation of  $2 h^{-1}\text{Mpc}$  exhibit higher intrinsic spin correlations (at  $3.1\sigma_b$  level) than those having ten or less neighbors within the same separation distance. This local density dependence of the galaxy spin correlations may be due to the stronger tidal forces from the denser environments.
- The observed spin correlation functions of the selected Scd galaxies follow the quadratic scaling with the linear density correlations, which is consistent with the prediction of the linear tidal torque theory.

We have also attempted to measure a luminosity dependence of the galaxy spin correlations by splitting the galaxy samples according to their absolute  $r$ -band magnitudes ( $M_r$ ), and noted that the correlation function has a peak at  $1.25 h^{-1}\text{Mpc}$  and  $2 h^{-1}\text{Mpc}$  for the fainter ( $M_r > -16.67$ ) and brighter sample ( $M_r \leq -16.67$ ), respectively. However, the two peaks from the two magnitude-split samples turn out to correspond to a similar angular separation, which hints at significant systematics. To make matters worse, the redshift distributions of the two magnitude-split samples

are found to be so different that it is impossible with our samples to disentangle a luminosity from a redshift dependence of the galaxy spin correlations. Therefore, we conclude that a luminosity dependence of the galaxy spin correlations cannot not be measured from our samples.

The behaviors of the detected correlations are found to be consistent with the predictions of the tidal torque theory. But, the correlation strength turns out to be greater than predicted by the numerical simulations. This result indicates that the spin orientations of the luminous galaxies are not aligned with those of the underlying dark halos and that the luminous galaxies retain better the initial memory of the tidally induced spin alignments than their dark counterparts. It is physically explained as the spin orientations of the luminous galaxies may be less vulnerable than those of their dark counterparts to the destructive nonlinear effects from the surroundings which tend to break the tidally induced intrinsic correlations. It has to be understood fully in the future how and under what circumstances the spin axes of the late-type spiral galaxies have retained their original orientations.

It is also worth mentioning the apparent inconsistency between our results and the previous studies which claimed that the two dimensional projected shapes of the blue SDSS galaxies show no correlation at higher redshifts,  $z \sim 0.1$ , (see e.g., Mandelbaum et al. 2010). Given that we have detected  $3.4\sigma$  correlation signal at  $z \leq 0.02$  and that the intrinsic spin correlations of the blue galaxies would be stronger at higher redshifts, one may naturally expect that the shape correlations of the blue galaxies at  $z \sim 0.1$  would be strong enough to affect the weak lensing signals, which is inconsistent with the previous results. We think of several reasons for this inconsistency: First, the two dimensional projected shapes of the blue galaxies may not be a good indicator of the tidally induced alignments; Second, there may be considerable uncertainties involved in the accurate measurements of the shape correlations of the blue galaxies at  $z \sim 0.1$ . As a final conclusion, our results will shed a new light on the study of the galaxy intrinsic alignments and the weak lensing analysis as well.

I thank M. Huertas-Company for providing information on the galaxy position angles and magnitudes. I also thank an anonymous referee for very useful comments which helped me improve significantly the original manuscript. This work was supported by the National Research Foundation of Korea (NRF) grant funded by the Korea government (MEST, No.2010-0007819). Support for this work was also provided by the National Research Foundation of Korea to the Center for Galaxy Evolution Research.

Funding for the SDSS and SDSS-II has been provided by the Alfred P. Sloan Foundation, the Participating Institutions, the National Science Foundation, the U.S. Department of Energy, the National Aeronautics and Space Administration, the Japanese Monbukagakusho, the Max Planck Society, and the Higher Education Funding Council for England. The SDSS Web Site is <http://www.sdss.org/>.

The SDSS is managed by the Astrophysical Research Consortium for the Participating Institutions. The Participating Institutions are the American Museum of Natural History, Astrophysical Institute Potsdam, University of Basel, University of Cambridge, Case Western Reserve University, University of Chicago, Drexel University, Fermi lab, the Institute for Advanced Study, the Japan Participation Group, Johns Hopkins University, the Joint Institute for Nuclear Astrophysics, the Kavli Institute for Particle Astrophysics and Cosmology, the Korean Scientist Group, the Chinese Academy of Sciences (LAMOST), Los Alamos National Laboratory, the Max-Planck-Institute for Astronomy (MPIA), the Max-Planck-Institute for Astrophysics (MPA), New Mexico State University, Ohio State University, University of Pittsburgh, University of Portsmouth, Princeton University, the United States Naval Observatory, and the University of Washington.

## REFERENCES

- Abazajian, K. N., et al. 2009, *ApJS*, 182, 543
- Aragón-Calvo, M. A., van de Weygaert, R., Jones, B. J. T., & van der Hulst, J. M. 2007, *ApJ*, 655, L5
- Aryal, B., & Saurer, W. 2005, *MNRAS*, 360, 125
- Altay, G., Colberg, J. M., & Croft, R. A. C. 2006, *MNRAS*, 370, 1422
- Avila-Reese, V., Firmani, C., & Hernández, X. 1998, *ApJ*, 505, 37
- Bailin, J., et al. 2005, *ApJ*, 627, L17
- Bailin, J. & Steinmetz, M. 2005, *ApJ*, 627, 647
- Bardeen, J. M., Bond, J. R., Kaiser, N., & Szalay, A. S. 1986, *ApJ*, 304, 15
- Bond, J. R., Kofman, L., & Pogosyan, D. 1996, *Nature*, 380, 603
- Brown, M. L., Taylor, A. N., Hambly, N. C., & Dye, S. 2002, *MNRAS*, 333, 501
- Catelan, P., Kamionkowski, M., & Blandford, R. D. 2001, *MNRAS*, 320, L7
- Catelan, P., & Theuns, T. 1996, *MNRAS*, 282, 436
- Crittenden, R. G., Natarajan, P., Pen, U. L & Theuns, T. 2001, *ApJ*, 559, 552
- Crittenden, R. G., Natarajan, P., Pen, U. L & Theuns, T. 2001, *ApJ*, 568, 20
- Croft, R. A. C. & Metzler, C. A. 2000, *ApJ*, 545, 561
- Doroshkevich, A. G. 1970, *Astrofizika*, 6, 581
- Dubinski, J. 1992, *ApJ*, 401, 441
- Erdoğdu, P., et al. 2006, *MNRAS*, 373, 45
- Fan, Z.-H. 2007, *ApJ*, 669, 10
- Flin, P., & Godlowski, W. 1986, *MNRAS*, 222, 525
- Fuller, T. M., West, M. J., & Bridges, T. J. 1999, *ApJ*, 519, 22 :: **infall/merging**
- Hahn, O., Porciani, C., Carollo, C. M., & Dekel, A. 2007, *MNRAS*, 375, 489
- Hahn, O., Teyssier, R., & Carollo, C. M. 2010, *MNRAS*, 405, 274
- Hambly, N. C., et al. 2001, *MNRAS*, 326, 1279

- Haynes, M. P. & Giovanelli, R. 1984, *AJ*, 89, 758
- Hartlap, J., Simon, P., & Schneider, P. 2007, *A&A*, 464, 399
- Heavens, A., Refregier, A., & Heymans, C. 2000, *MNRAS*, 319, 649
- Heymans, C. & Heavens, A. 2003, *MNRAS*, 339, 711
- Hirata, C. M. & Seljak, U. 2004, *Phys. Rev. D*, 70, 063526
- Hirata, C. M., et al. 2004, *MNRAS*, 353, 529
- Hirata, C. M., et al. 2007, *MNRAS*, 381, 1197
- Huertas-Company, M., Aguerra, J. A. L, Bernardi, M., Mei, S., & Sánchez Almeida, J. 2010, arXiv:1010.3018
- Hui, L. & Zhang Z. 2002, preprint [astro-ph/0205512]
- Hui, L., & Zhang, J. 2008, *ApJ*, 688, 742
- Jimenez, R., Padoan, P., Matteucci, F. & Heavens, A. F. 1998, *MNRAS*, 299, 123
- Jing, Y. 2002, *MNRAS*, 335, L89
- Joachimi, B., & Bridle, S. L. 2010, *A&A*, 523, A1
- Joachimi, B., Mandelbaum, R., Abdalla, F. B., & Bridle, S. L. 2010, arXiv:1008.3491
- Jones, B. J. T., van de Weygaert, R., & Aragón-Calvo, M. A. 2010, *MNRAS*, 408, 897
- King, L. 2005, *A&A*, 441, 47
- Komatsu, E. et al. 2010, *ApJS*, 192, 18
- Lee, J. & Pen, U. L. 2000, *ApJ*, 532, L5
- Lee, J. & Pen, U. L. 2001, *ApJ*, 555, 106
- Lee, J. & Pen, U. L. 2002, *ApJ*, 567, 111
- Lee, J. 2006, *ApJ*, 644, L5
- Lee, J. & Erdogdu, P. 2007, 671, 1248
- Lee, J., & Pen, U.-L. 2007, *ApJ*, 670, L1
- Lee, J., & Pen, U.-L. 2008, *ApJ*, 681, 798
- Lee, J., Springel, V., Pen, U.-L., & Lemson, G. 2008, *MNRAS*, 389, 1266

- Lee, J., Hahn, O., & Porciani, C. 2009, *ApJ*, 707, 761
- Lupton, R. H., Gunn, J. E., & Szalay, A. S. 1999, *AJ*, 118, 1406
- Mackey, J., White, M., & Kamionkowski, M. 2002, *MNRAS*, 332, 788
- Mandelbaum, R., Hirata, C. M., Ishak, M., Seljak, U., & Brinkmann, J. 2006, *MNRAS*, 367, 611
- Mandelbaum, R., et al. 2010, *MNRAS*, 1486
- Mo, H. J., Mao, S. & White, S. D. M. 1998, *MNRAS*, 295, 319
- Navarro, J.F., Abadi, M.G., & Steinmetz, M. 2004, *ApJ*, 613, L41
- Patiri, S. G., Cuesta, A. J., Prada, F., Betancort-Rijo, J., & Klypin, A. 2006, *ApJ*, 652, 75
- Paz, D. J., Stasyszyn, F., & Padilla, N. D. 2008, *MNRAS*, 389, 1127
- Peebles, P. J. E. 1969, *ApJ*, 155, 393
- Pen, U. L., Lee, J., & Seljak, U. 2000, 543, L107
- Porciani, C., Dekel, A., & Hoffman, Y. 2002, *MNRAS*, 332, 339
- Saunders, W., et al. 2000, *MNRAS*, 317, 55
- Schäfer, B. M. 2009, *International Journal of Modern Physics D*, 18, 173
- Schneider, M. D., & Bridle, S. 2010, *MNRAS*, 402, 2127
- Slosar, A., et al. 2009, *MNRAS*, 392, 1225
- Springel, V., et al. 2005, *Nature*, 435, 629
- Sugerman, B., Summers, F. J., & Kamionkowski, M. 2000, *MNRAS*, 311, 762
- Trujillo, I., Carretero, C., & Patiri, S. 2006, *ApJ*, 610, L111
- White, S. D. M. 1984, *ApJ*, 286, 38
- York, D. G., et al. 2000, *AJ*, 120, 1579

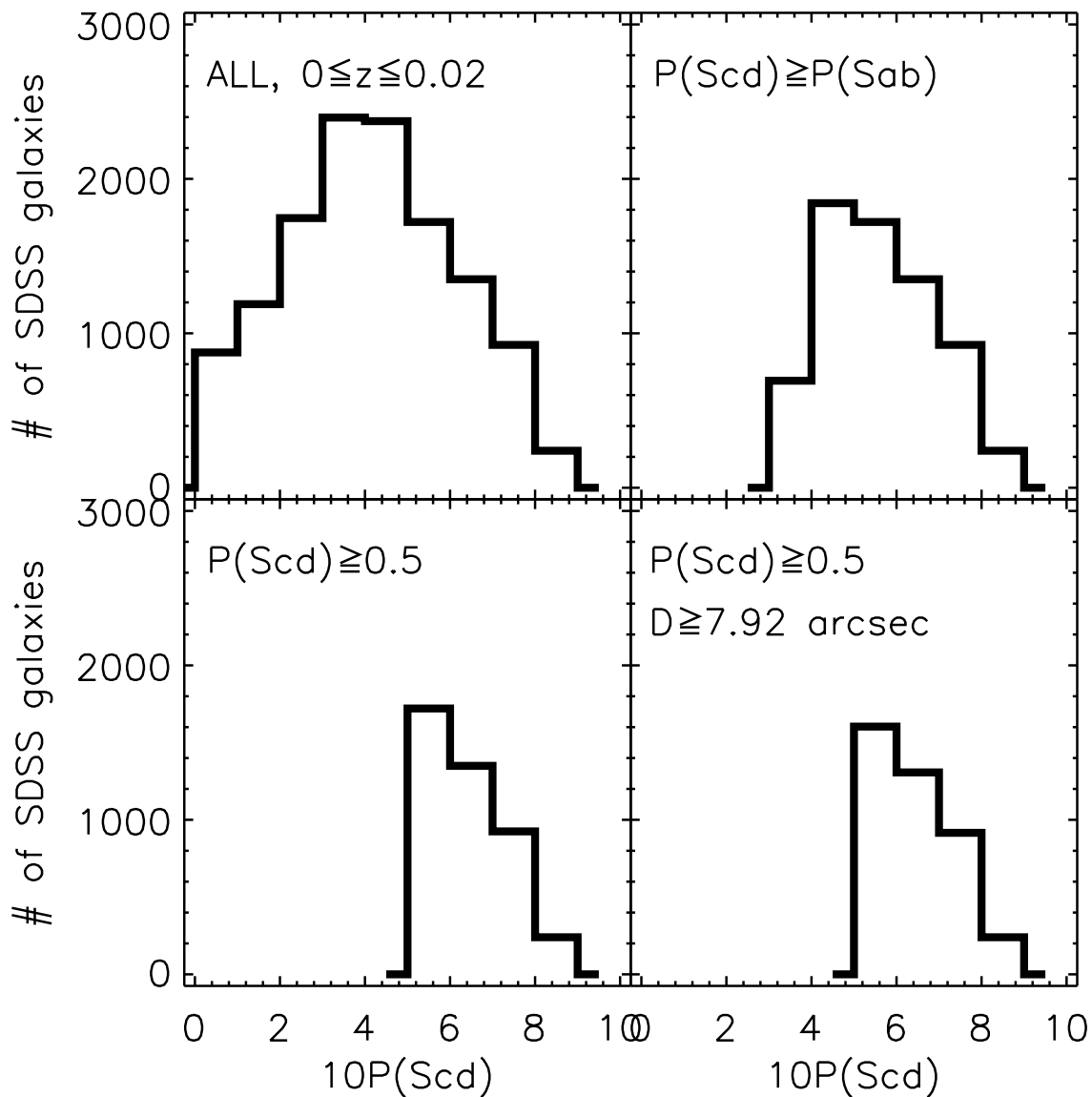


Fig. 1.— Number distribution of the nearby galaxies ( $0 \leq z \leq 0.02$ ) from the SDSS DR7 as a function of  $P(\text{Scd})$ , the probability of being classified as Scd galaxies for four different cases: all nearby galaxies (top left panel);  $P(\text{Scd})$  is largest (top right panel);  $P(\text{Scd}) \geq 0.5$  (bottom left panel); with diameter larger than  $20h^{-1}\text{Kpc}$  and  $P(\text{Scd}) \geq 0.5$  (bottom right panel).

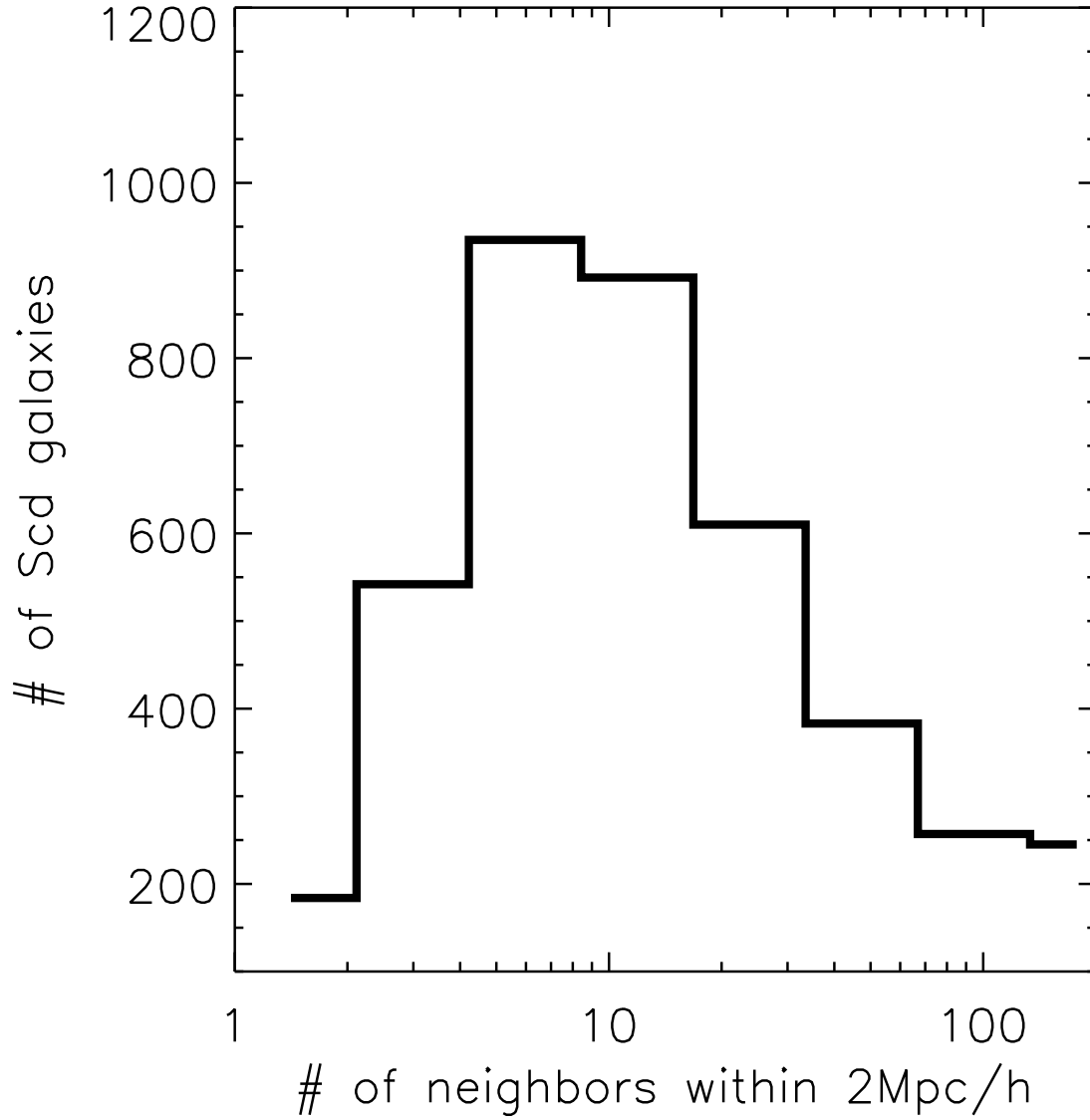


Fig. 2.— Number distribution of the selected Scd galaxies from the SDSS DR7 as a function of the number of neighbor galaxies located within the separation distance of  $2 h^{-1} \text{Mpc}$  at  $0 \leq z < 0.02$ .

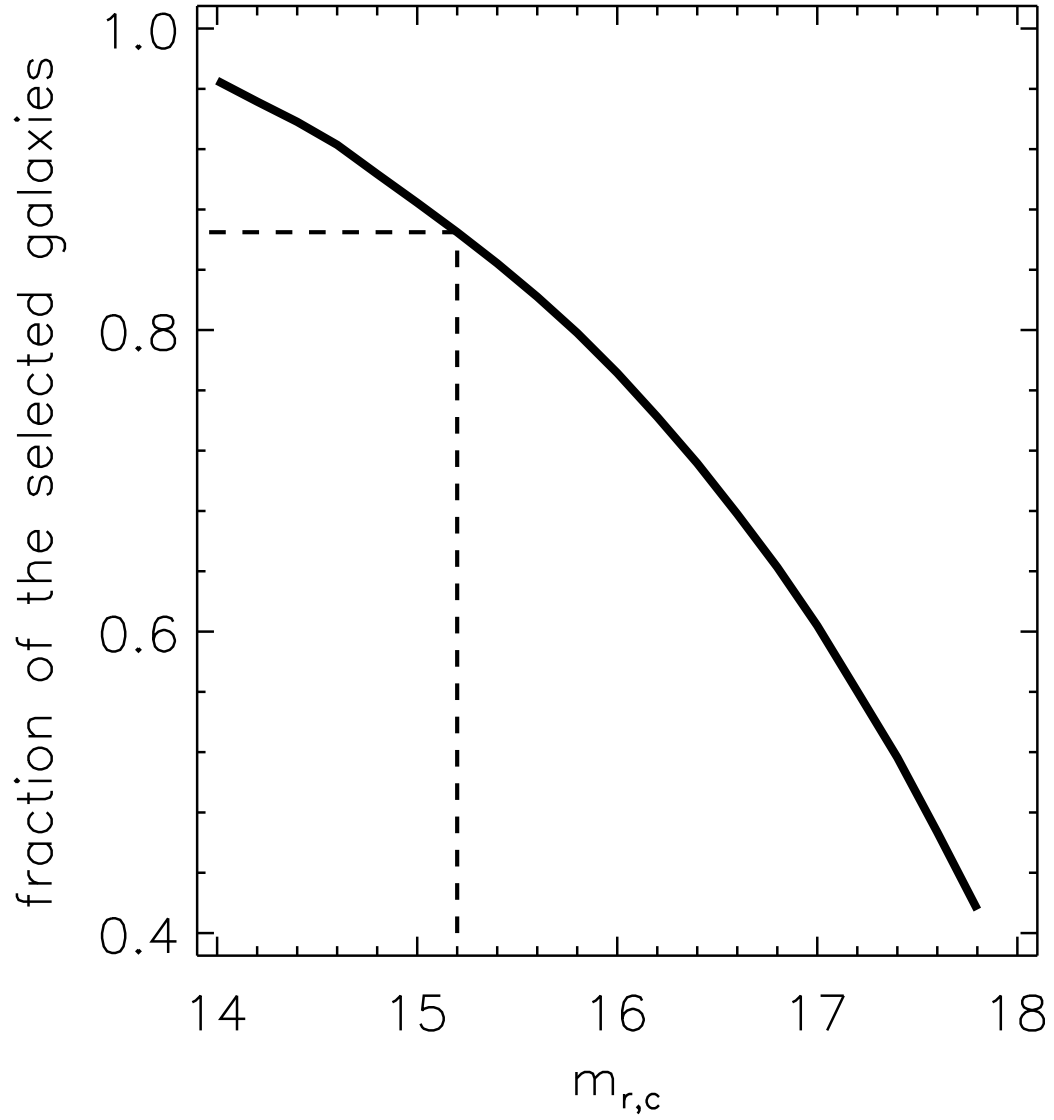


Fig. 3.— Fraction of the galaxies belonging to the volume-limited SDSS sample as a function of the  $r$ -band magnitude limit,  $m_{r,c}$ . The dashed line corresponds to the applied magnitude cut.

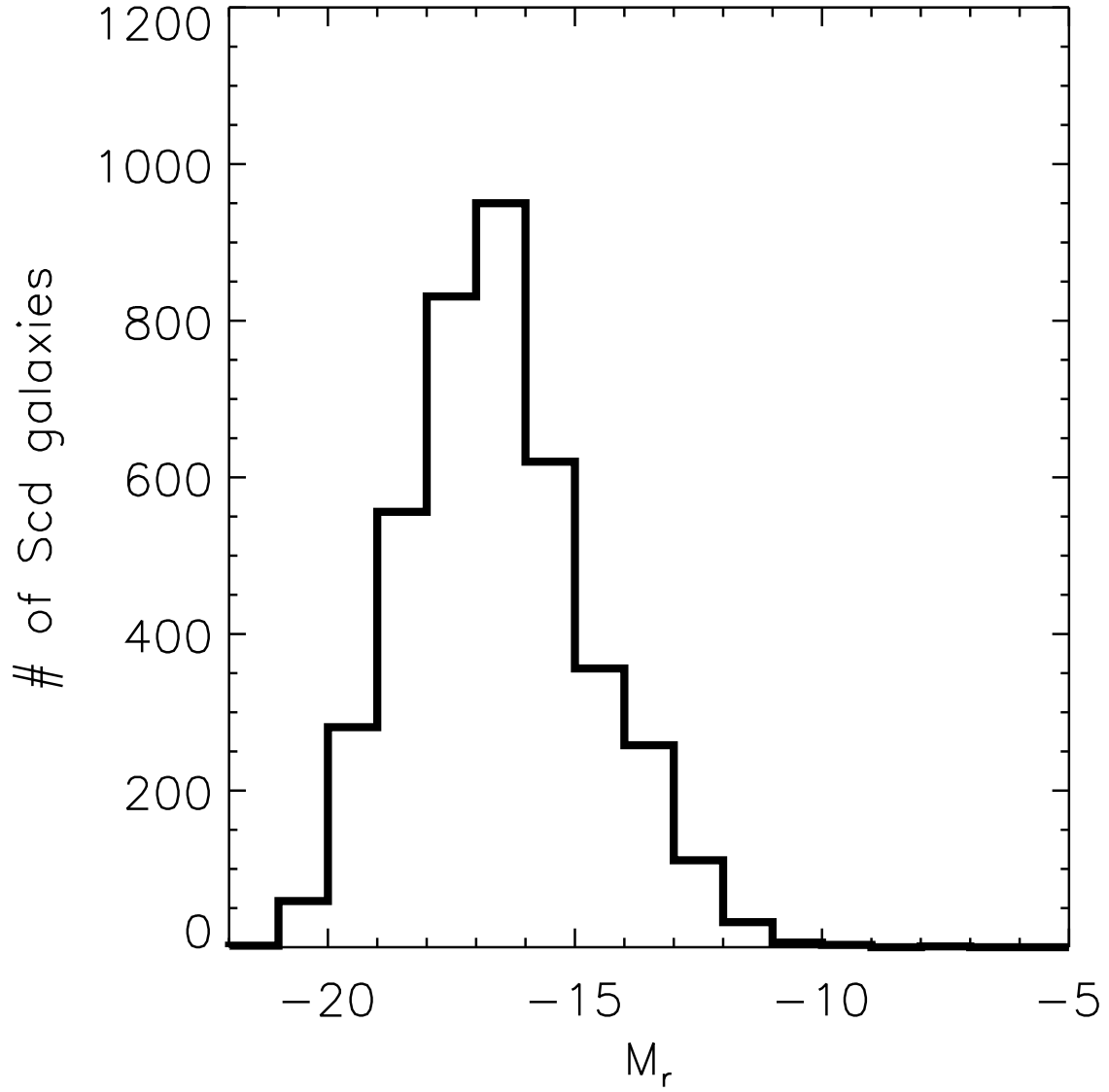


Fig. 4.— Number distribution of the selected Scd galaxies from the SDSS DR7 as a function of the r-band absolute magnitude at  $0 \leq z < 0.02$ .

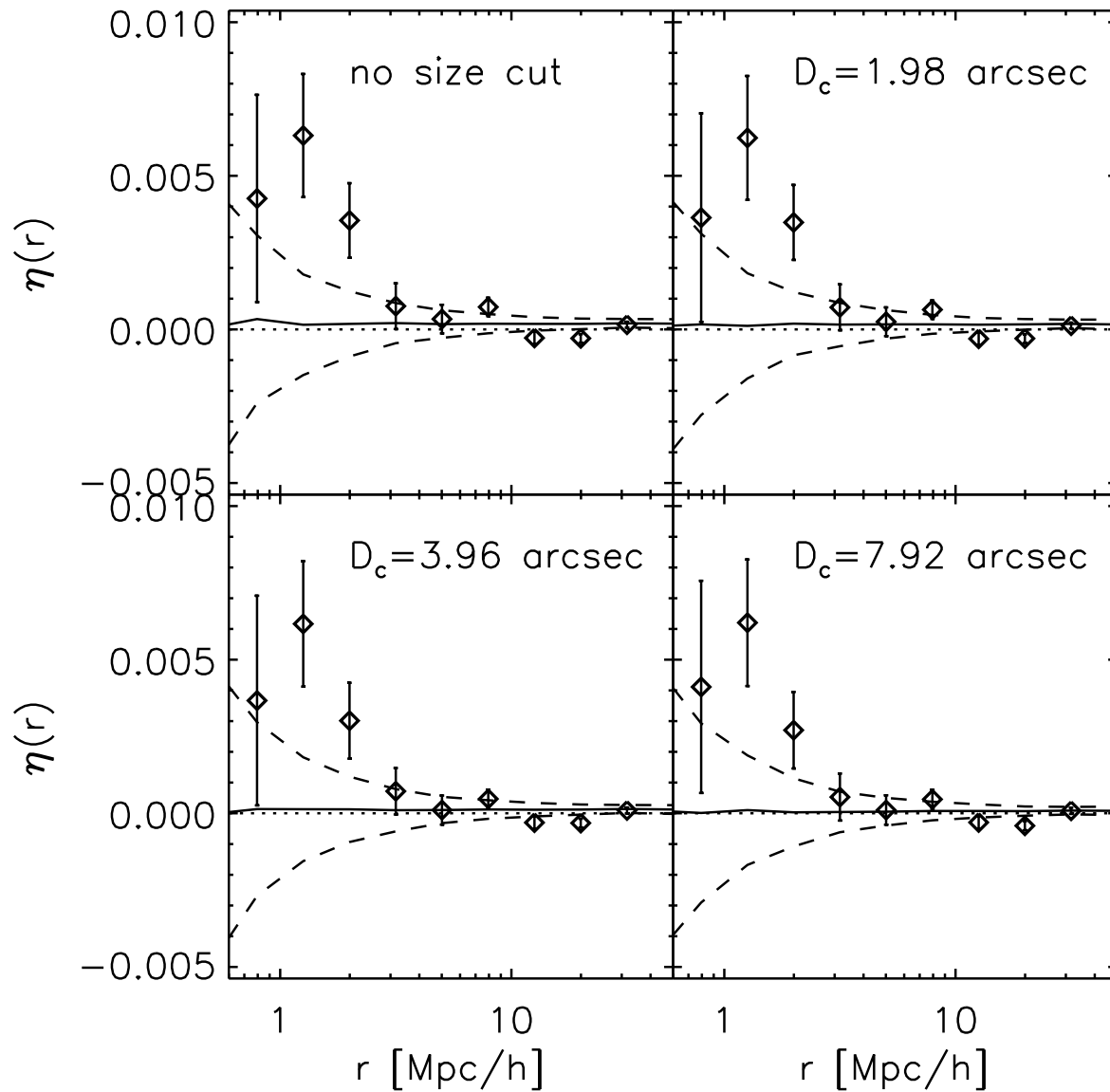


Fig. 5.— Correlations of the unit spin vectors of the selected Scd galaxies (diamond dots) as a function of the separation distance  $r$  at  $0 \leq z < 0.02$  for the four different cases of the galaxy diameter cut,  $D_c$ . In each panel, the thin solid line represents the mean correlation averaged over the 1000 bootstrap resamples, the dashed lines represent one standard deviation among the bootstrap resamples, and the dotted line indicates the zero correlation signal.

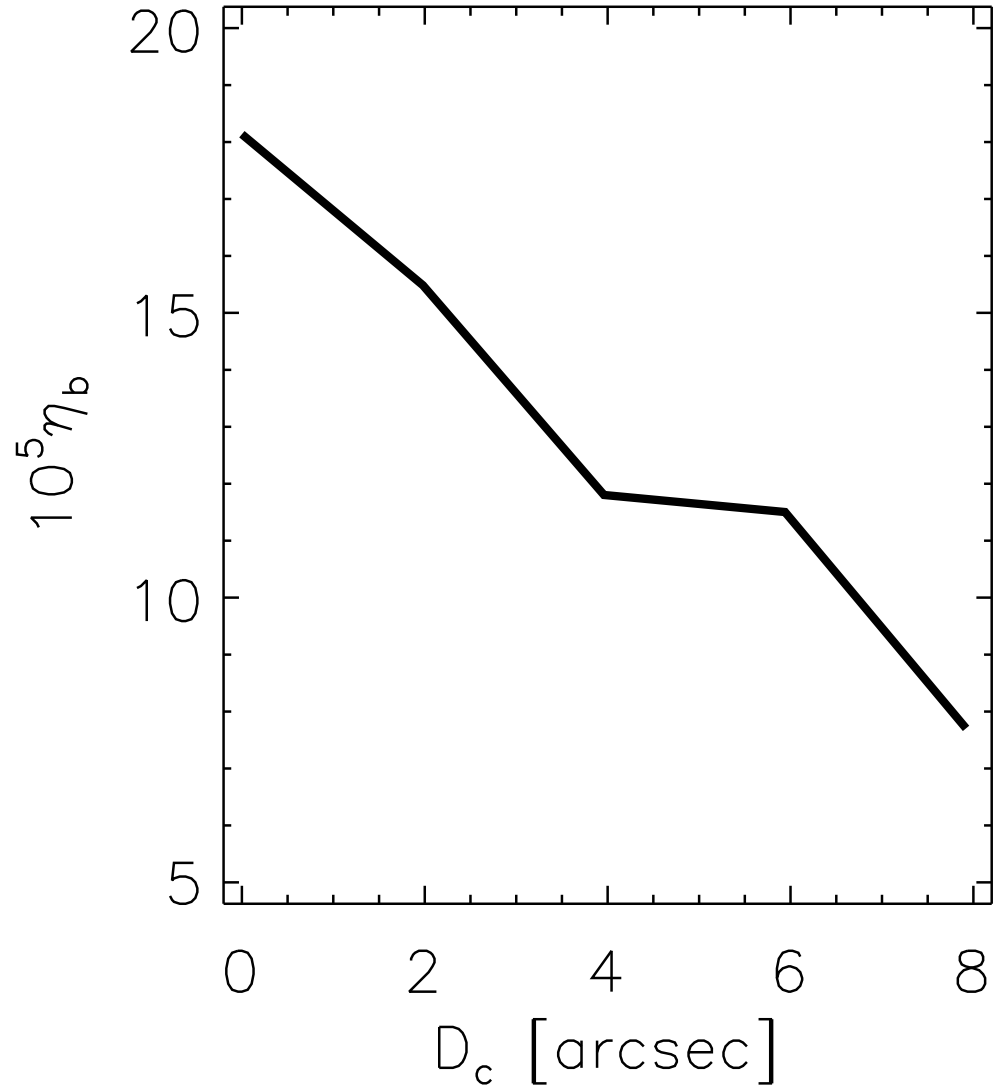


Fig. 6.— Bootstrap mean averaged over the 1000 bootstrap resamples measured at  $r \sim 10 h^{-1} \text{Mpc}$ , as a function of  $D_c$ .

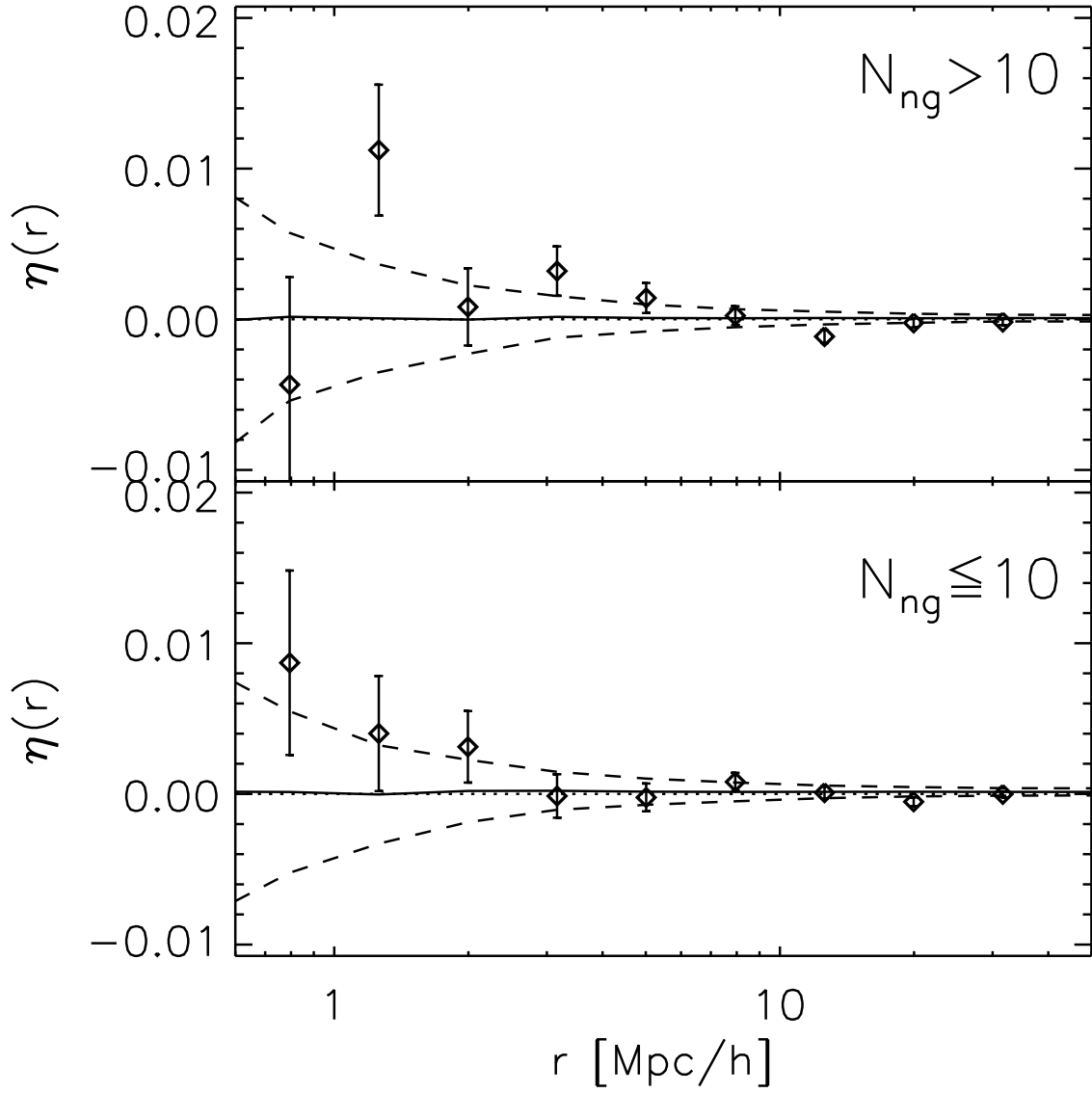


Fig. 7.— Same as Figure 5 but using only those Scd galaxies which have more (less) than  $N_{ng,c} = 10$  neighbor galaxies within separation  $r_s = 2 h\text{Mpc}$  in the upper (lower) panel.

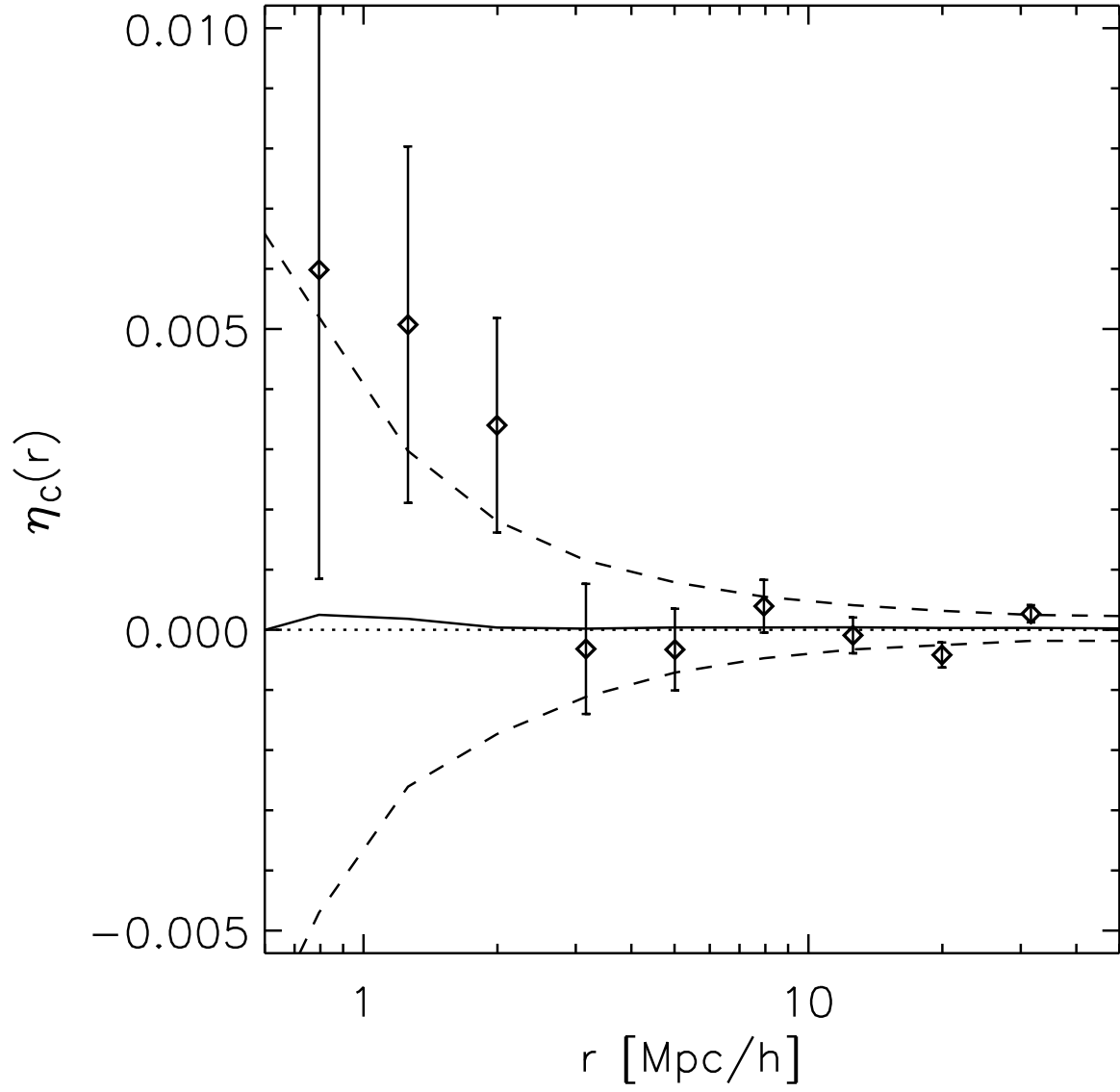


Fig. 8.— Same as Figure 8 but between the Scd galaxies having more than 10 neighbors and the Scd galaxies having less than 10 neighbors.

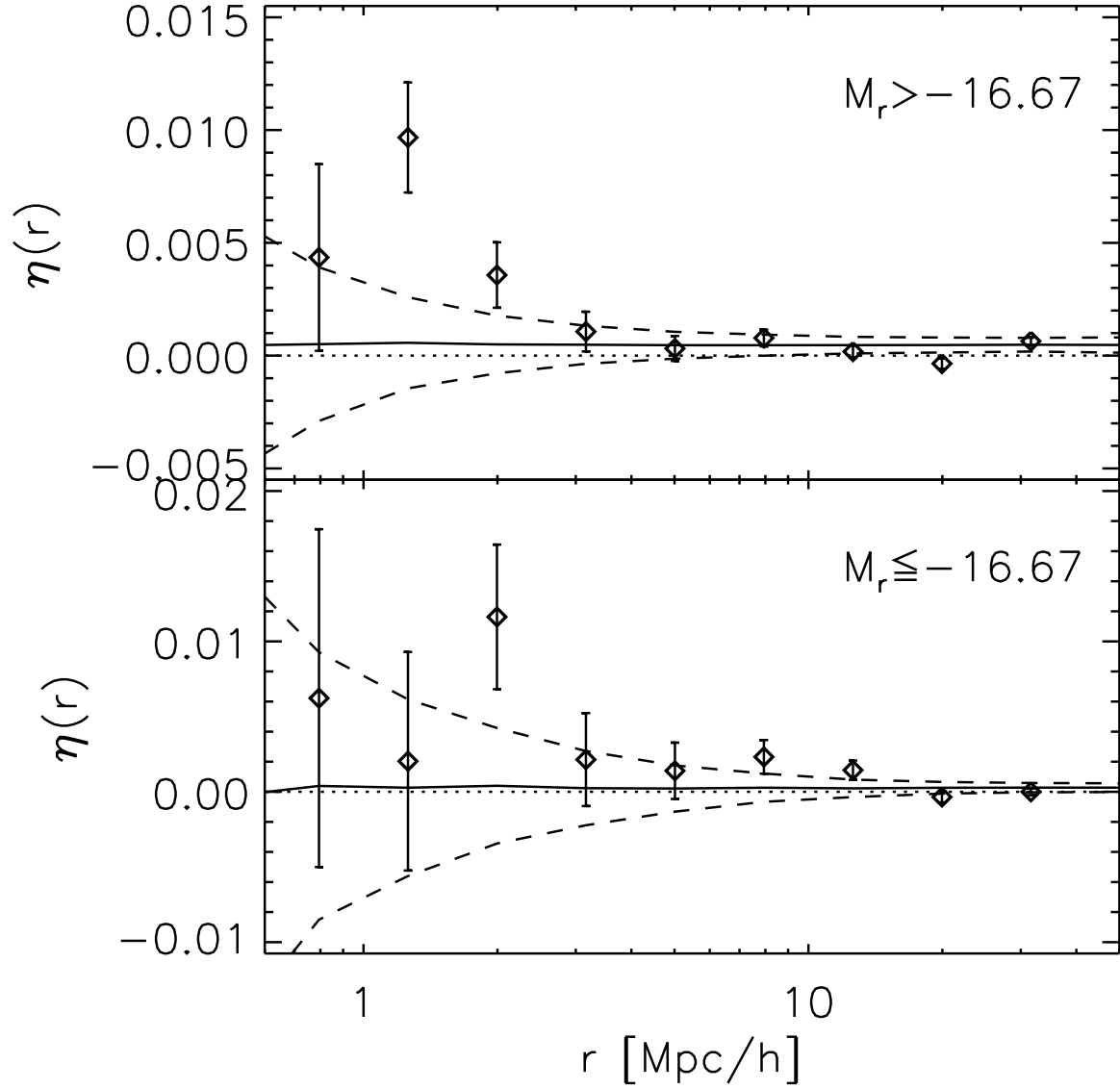


Fig. 9.— Same as Figure 5 but using only those Scd galaxies which are fainter (brighter) than  $M_{r,c} = -16.67$  in the upper (lower) panel.

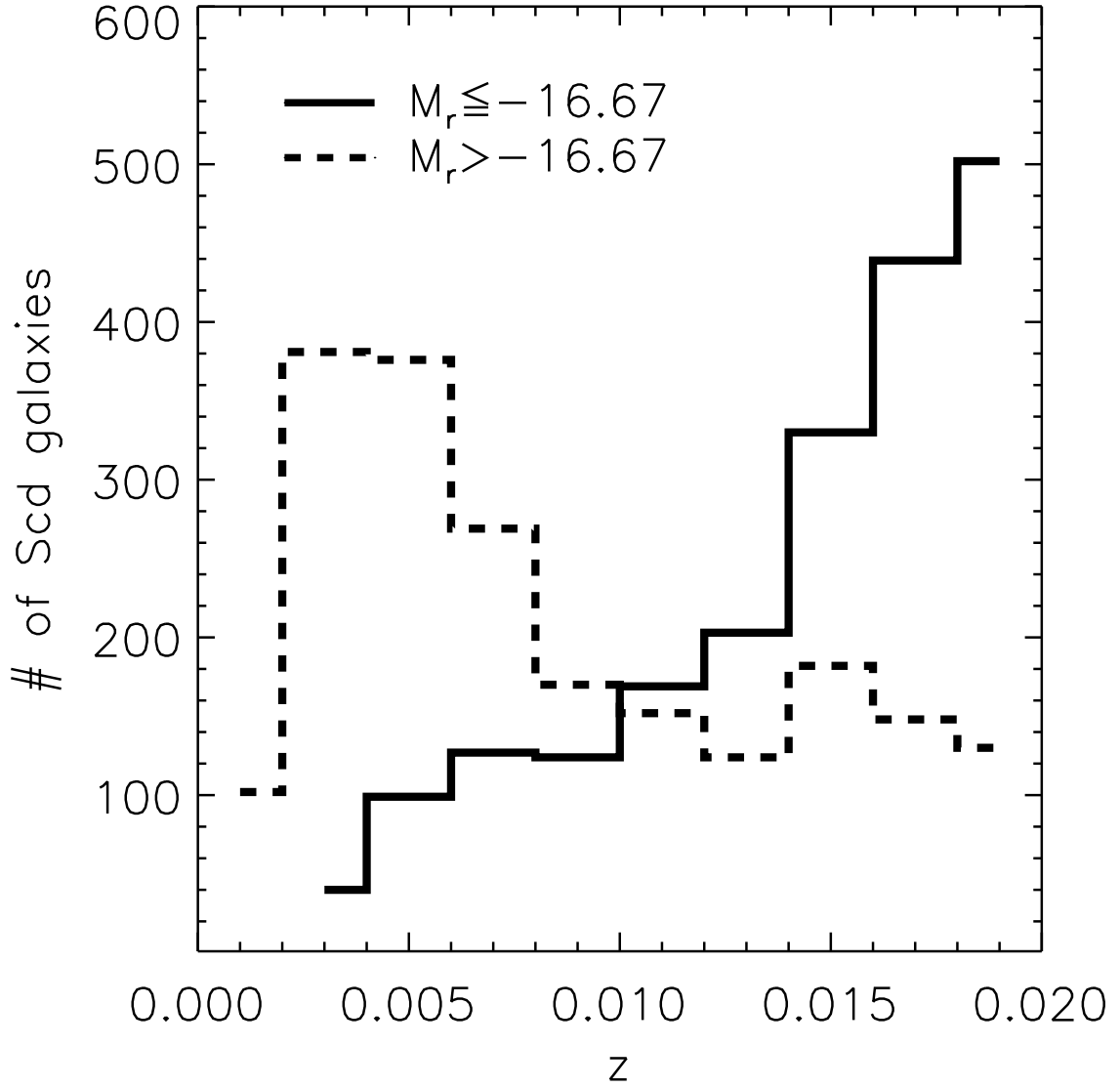


Fig. 10.— Redshift distribution of the fainter galaxy sample (dashed line) and bright galaxy sample (solid line).

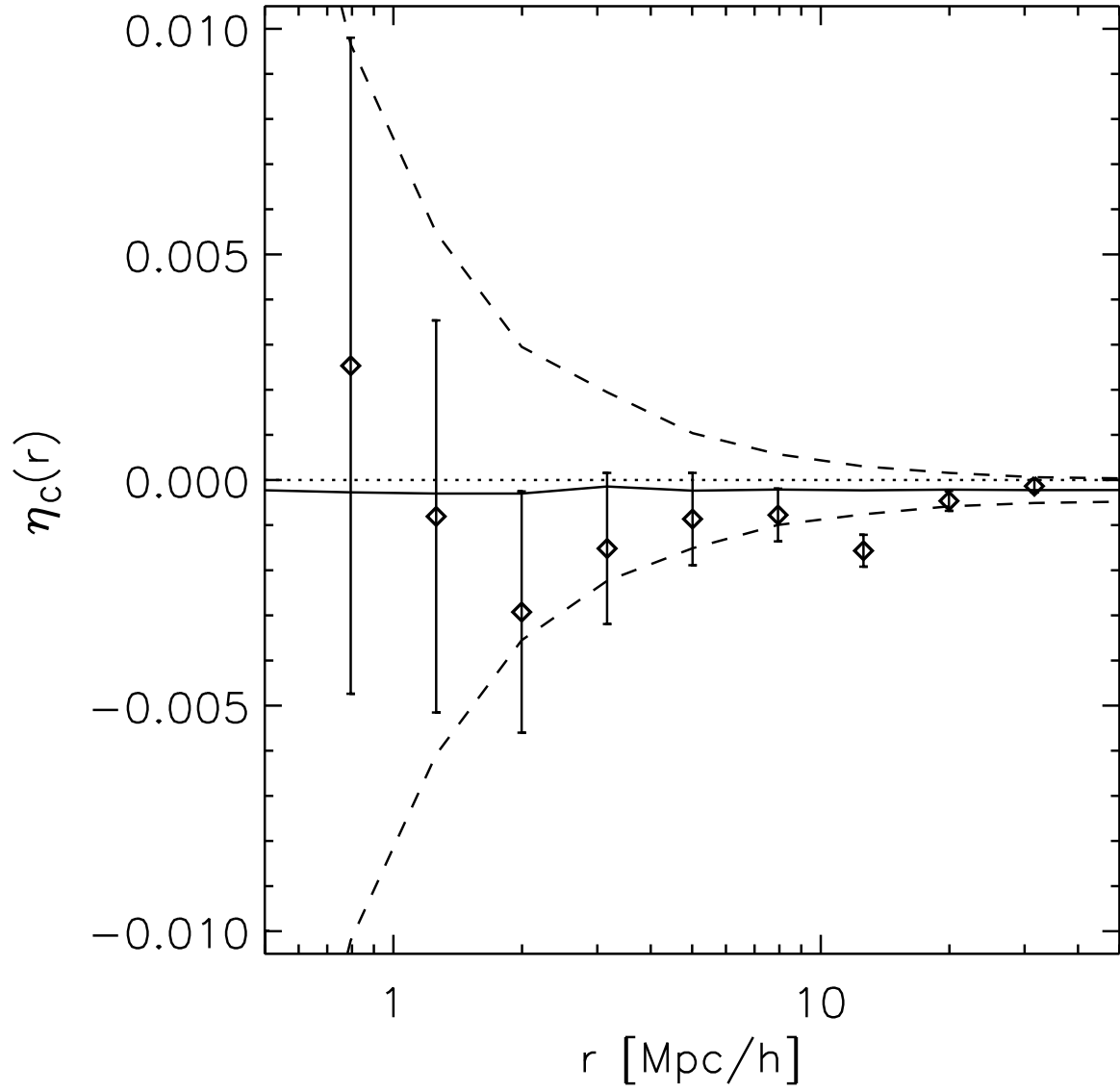


Fig. 11.— Cross-correlations of the unit-spin vectors between the faint and the bright Scd galaxies at  $0 \leq z < 0.02$ .

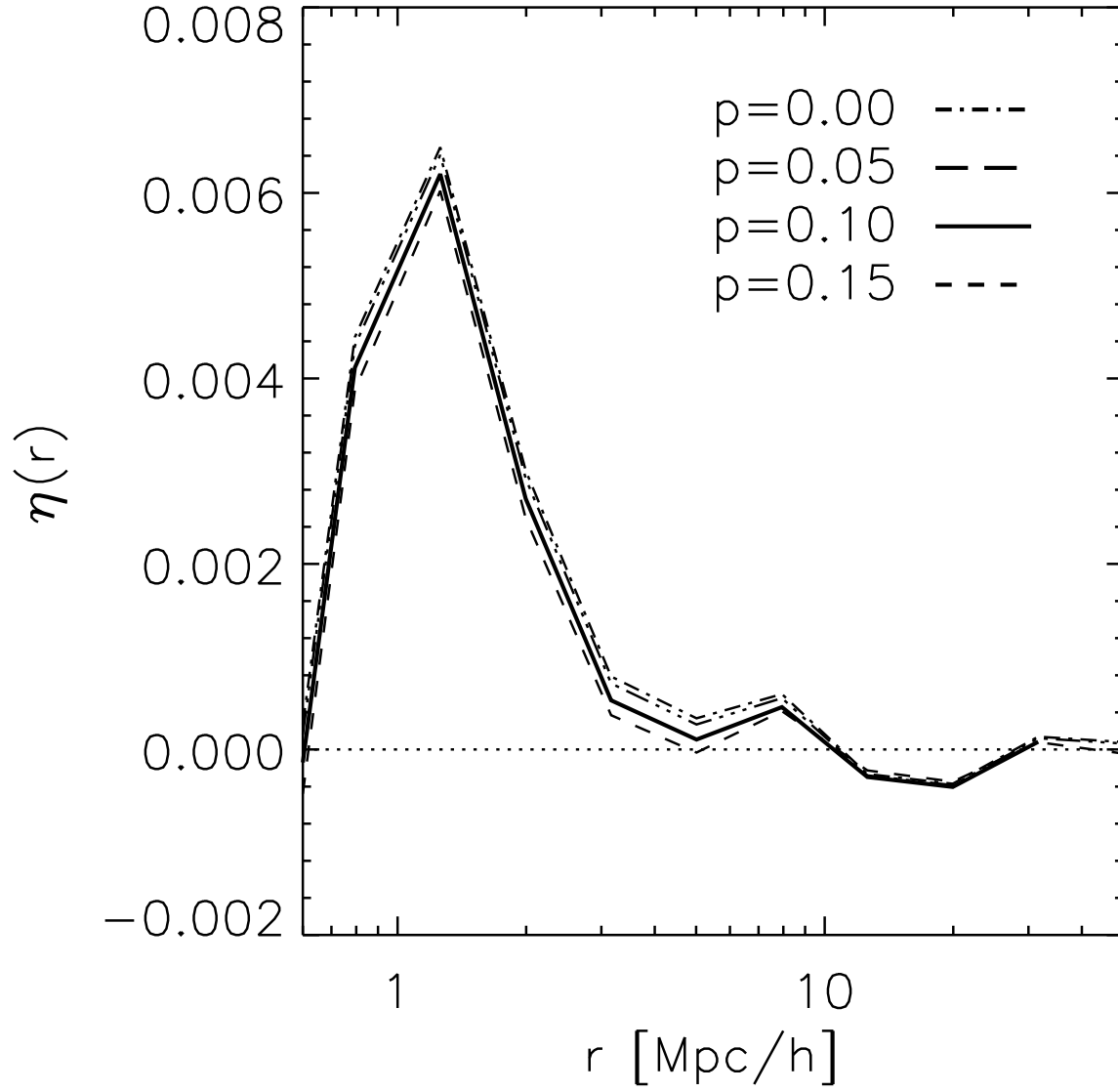


Fig. 12.— Same as the bottom-right panel of Figure 5 but for four different values of the intrinsic flatness parameter,  $p$ .

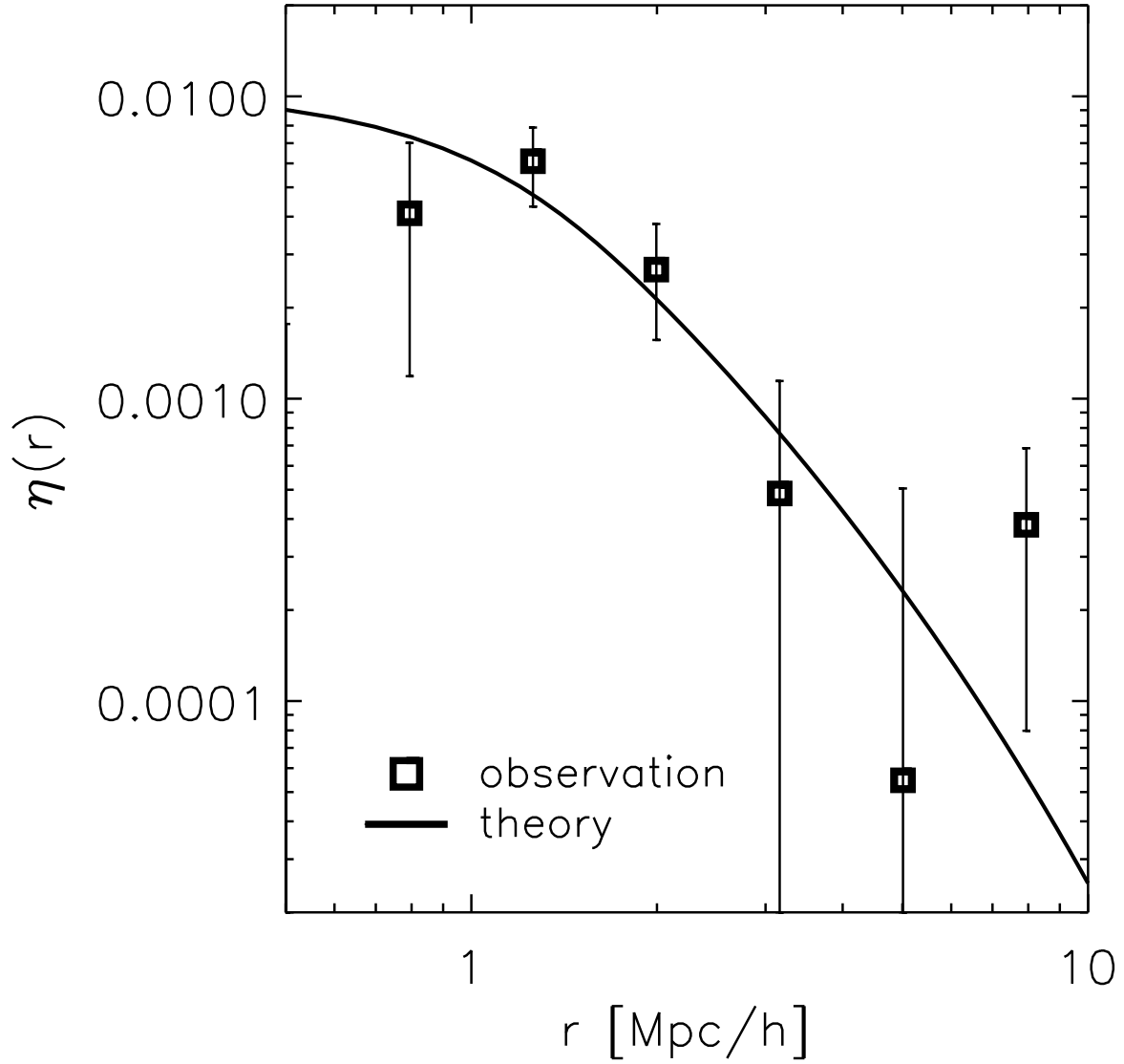


Fig. 13.— Comparison of the spin-correlations of the selected Scd galaxies (square dots) with the theoretical model with the best-fit parameter (solid line). The data points (square dots) are obtained by subtracting the bootstrap average from the observed spin-correlation values. The errors represents  $1\sigma$  bootstrap scatter.

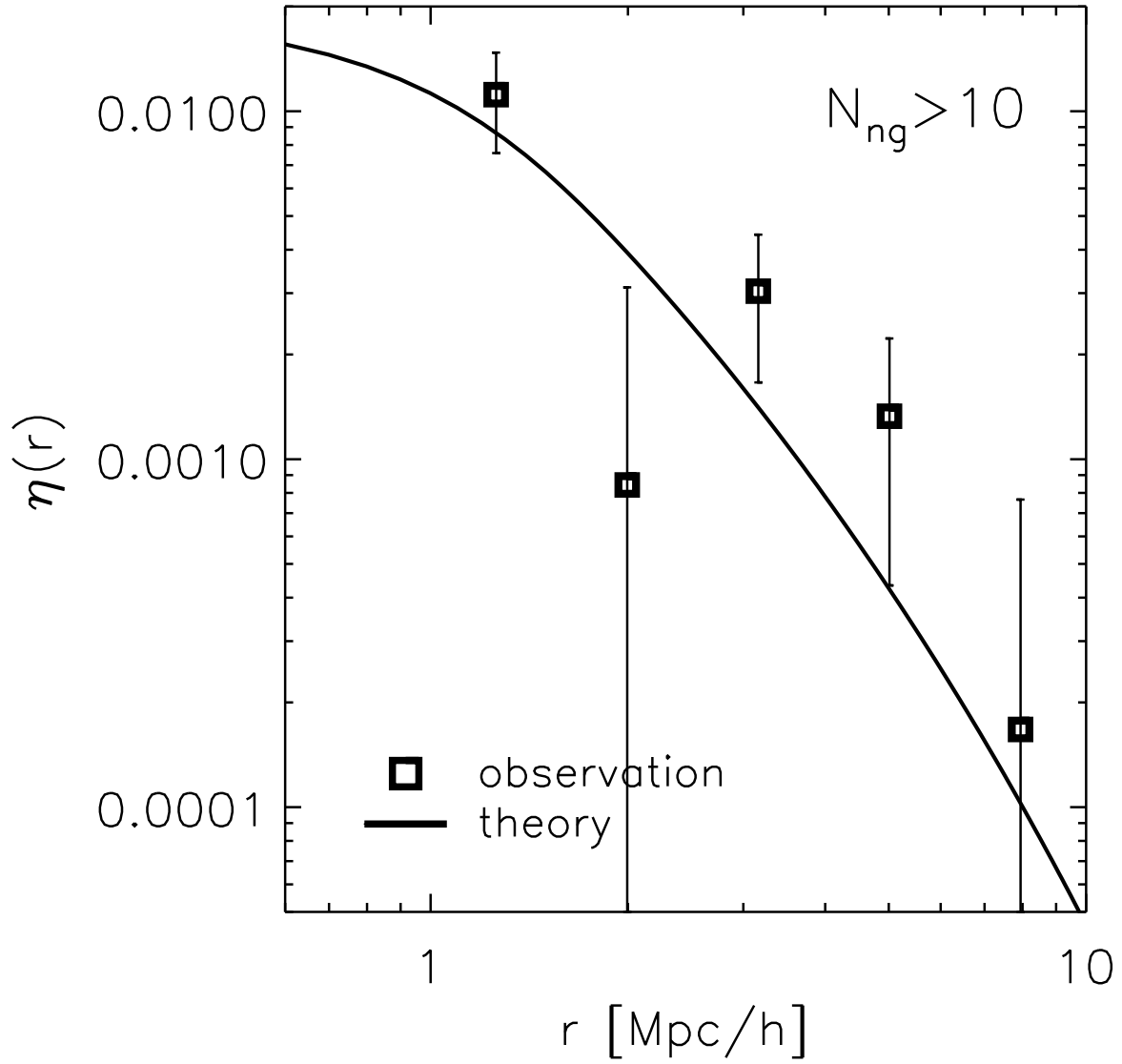


Fig. 14.— Same as Figure 13 but only for those Scd galaxies with  $N_{ng} > 10$ .

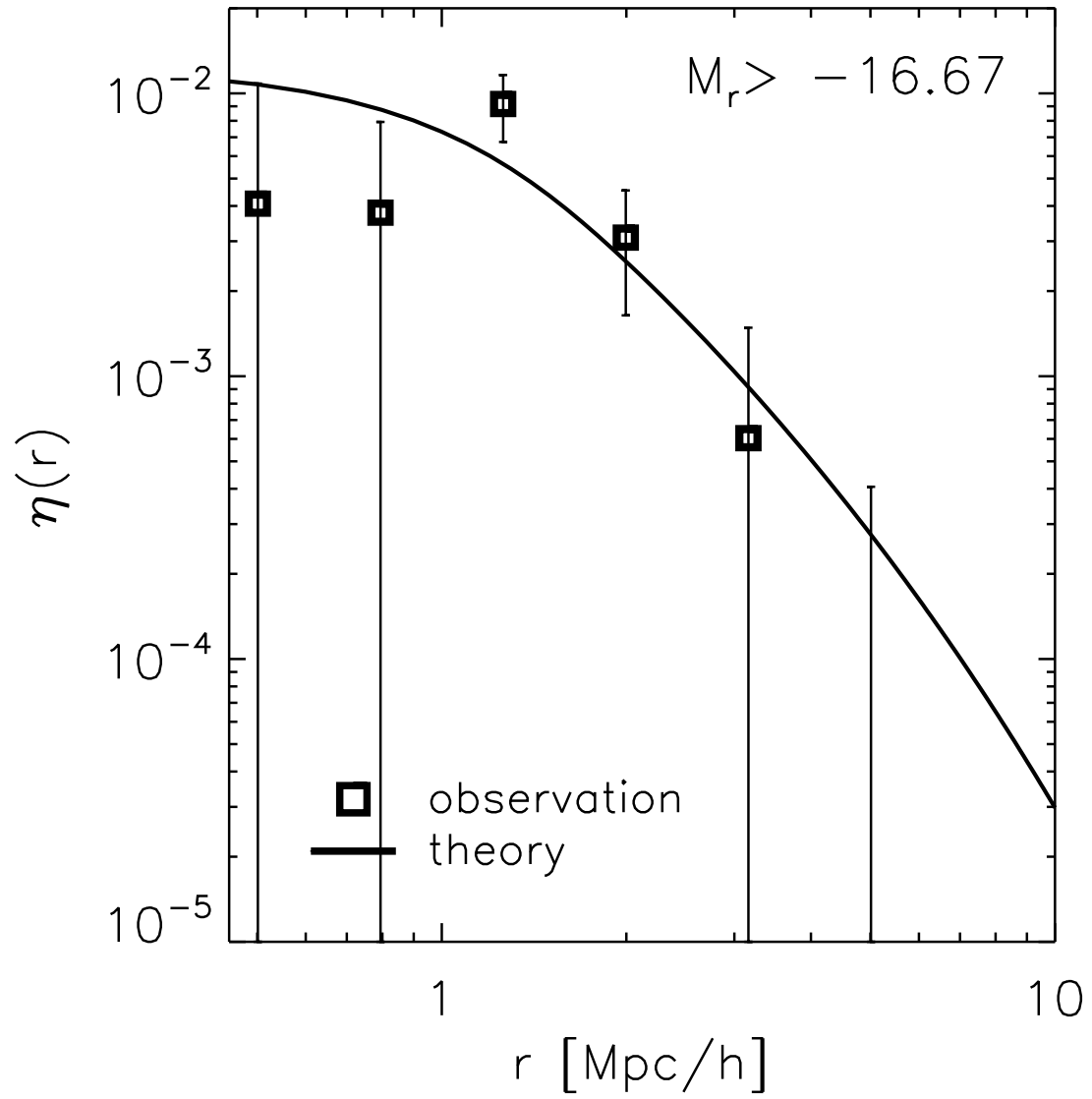


Fig. 15.— Same as Figure 13 but only for those Scd galaxies with  $M_r > -16.67$ .

Table 1. number of the selected Scd galaxies, mean redshift, mean  $r$ -band absolute magnitude, and mean number of neighbor galaxies within  $r_s$ .

$N_{\text{Scd}}$	$\bar{z}$	$\bar{M}_r$	$\bar{N}_{ng}$
4067	0.01	–16.56	27

Table 2. selection condition, number of the galaxies, median redshift, and the mean redshift

condition	$N_g$	$z_m$	$\bar{z}$ .
$M_r > -16.67$	2034	0.007	0.009
$M_r \leq -16.67$	2033	0.015	0.014

Table 3. selection condition, number of the galaxies, best-fit value of  $a$ , reduced  $\chi^2$ .

condition	$N_g$	$a$	$\chi_r^2$
—	4067	$0.25 \pm 0.04$	0.83
$N_{ng} > 10$	1945	$0.34 \pm 0.07$	1.10
$M_r > -16.67$	2034	$0.27 \pm 0.04$	1.87